Chapter 2
Battery Cathodes

Marca M. Doeff

Glossary

Anode – (negative electrode)	This electrode donates electrons during cell discharge.
Battery	A device consisting of one or many electrochemical cells connected together, in which chemical energy is converted into power. These can be further categorized as primary (non-rechargeable) or secondary (rechargeable) systems.
Capacity	The amount of charge that a battery contains, often expressed as mAh or Ah. This depends on the size of the battery and its chemistry. Rated capacity also depends on the current used.
Cathode – (positive electrode)	This electrode accepts electrons during cell discharge.
Cell	One unit of a battery, commonly consisting of an anode, a cathode, an electrolyte, a separator, and two current collectors.
Energy density or specific energy	Energy per unit volume or weight of a material or a device, respectively, often expressed as Wh/L or Wh/kg. Energy is a product of the cell voltage and capacity per unit volume or weight.

This chapter was originally published as part of the Encyclopedia of Sustainability Science and Technology edited by Robert A. Meyers. DOI:10.1007/978-1-4419-0851-3

M.M. Doeff (✉)
Environmental Energy Technologies Division, Lawrence Berkeley National Laboratory,
University of California, Berkeley, CA 94720, USA
e-mail: mmdoeff@lbl.gov

R.J. Brodd (ed.), *Batteries for Sustainability: Selected Entries from the Encyclopedia of Sustainability Science and Technology*, DOI 10.1007/978-1-4614-5791-6_2,

Intercalation compound (host material, insertion compound)	Originally, this referred specifically to layered structures that can undergo insertion of ions or molecules between the van der Waals gaps, but is now commonly used for any structure that undergoes topotactic insertion reactions. For Li-ion battery materials, it refers specifically to compounds that undergo reductive insertion of lithium ions, such as graphite (used as an anode) or $LiCoO_2$ (used as a cathode).
Jahn–Teller effect	The geometric distortion of nonlinear complexes of certain transition metal ions to remove degeneracy. For example, Mn(III) in octahedral coordination is expected to have an electronic configuration of $t_{2g}{}^3e_g{}^1$. Elongation along one axis of the octahedron, for example, decreases the symmetry and removes the degeneracy.
Power density and specific power	Power per unit volume or weight, respectively, often expressed as W/L or W/kg. Power is the product of the current and the operating voltage. This is a function both of the materials used and the cell design.
Practical energy density or specific energy	Based on the entire weight or volume of the device including inert components. It may be only 1/4–1/2 of the theoretical energy density. It may also refer only to the useable portion of the theoretical capacity of the anode or cathode material itself.
Ragone plot	A plot showing the relationship between energy density and power density for any particular battery chemistry. This relationship is a function both of battery design and chemistry for Li-ion batteries.
Solid electrolyte interface (SEI)	A very thin (nanometer scale) layer formed on a lithium or lithiated graphite anode, which develops upon reaction with certain kinds of electrolytic solutions. The SEI is a specific kind of reaction layer that is ionically conductive but electronically insulating. It passivates the electrode, preventing further reaction with the electrolytic solution, and allows reversible operation of the device.
Specific capacity	The amount of charge per unit weight that a battery electrode material contains, often expressed as mAh/g. This is a fundamental characteristic of the material, and depends upon its redox chemistry and structure.

Theoretical energy density, specific energy, capacity	Based on weight or volume of the electrode active materials only.
Topotactic transformation	A transformation in a crystal lattice involving displacement or exchange of atoms, which maintains the basic structure.

Definition of the Subject and Its Importance

In a discharging battery, the cathode is the positive electrode, at which electrochemical reduction takes place. As current flows, electrons from the circuit and cations from the electrolytic solution in the device move toward the cathode. Although these processes are reversed during cell charge in secondary batteries, the positive electrode in these systems is still commonly, if somewhat inaccurately, referred to as the cathode, and the negative as the anode. Because this terminology is widespread throughout the Li-ion battery literature, this usage will be adopted for this article.

Li-ion batteries are dual intercalation systems, in which both the cathode and the anode have structures that allow reversible insertion and extraction of lithium cations. In principle, there are numerous materials that undergo reversible intercalation and can serve as electrode materials. Hence the chemistry of the Li-ion battery is not fixed, unlike the great majority of battery systems. The choice of cathode greatly affects the performance and cost of a Li-ion battery; for example, it is a major determinant of energy density, since it typically has a lower specific capacity than the most common anode material, graphite (372 mAh/g), to which it must be matched.

Introduction

The very high theoretical capacity of lithium (3,829 mAh/g) provided a compelling rationale from the 1970s onward for the development of rechargeable batteries employing the elemental metal as an anode. The realization that some transition metal compounds undergo reductive lithium intercalation reactions reversibly allowed the use of these materials as cathodes in these devices, most notably, TiS_2 [1–3]. Another intercalation compound, $LiCoO_2$, was described shortly thereafter [4, 5] but, because it was produced in the discharged state, was not considered to be of interest by battery companies at the time.

Due to difficulties with the rechargeability of lithium and related safety concerns, however, alternative anodes were sought. The graphite intercalation compound (GIC) LiC_6 was considered an attractive candidate [6] but the high reactivity with commonly used electrolytic solutions containing organic solvents

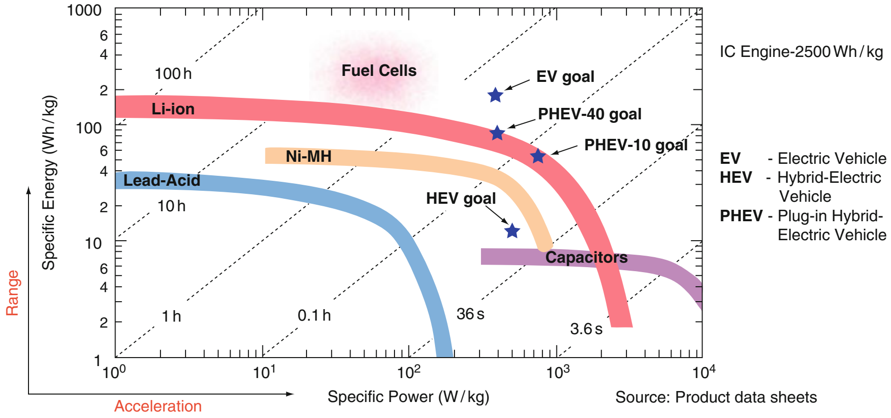

Fig. 2.1 A Ragone plot, showing the relationship between specific power and specific energy for several types of electrochemical devices. Goals set by FreedomCar for HEV, PHEVs, and EVs are also indicated (Used with permission from [10])

was recognized as a significant impediment to its use. The development of electrolytes that allowed the formation of a solid electrolyte interface (SEI) on surfaces of the carbon particles was a breakthrough that enabled commercialization of Li-ion batteries [7]. In 1990, Sony announced the first commercial batteries based on a dual Li-ion intercalation system [8]. These devices are assembled in the discharged state, so that it is convenient to employ a prelithiated cathode such as $LiCoO_2$ with the commonly used graphite anode. After charging, the batteries are ready to power devices.

The practical realization of high energy density Li-ion batteries revolutionized the portable electronics industry, as evidenced by the widespread market penetration of mobile phones, laptop computers, digital music players, and other lightweight devices, since the early 1990s. In 2009, worldwide sales of Li-ion batteries for these applications alone were US$7 billion [9]. Furthermore, their performance characteristics (Fig. 2.1) make them attractive for traction applications such as hybrid electric vehicles (HEVs), plug-in hybrid electric vehicles (PHEVs), and electric vehicles (EVs); a market predicted to be potentially ten times greater than that of consumer electronics. In fact, only Li-ion batteries can meet the requirements for PHEVs as set by the US Advanced Battery Consortium (USABC), although they still fall slightly short of EV goals.

In the case of Li-ion batteries, the trade-off between power and energy shown in Fig. 2.1 is a function both of device design and the electrode materials that are used. Thus, a high-power battery (e.g., one intended for an HEV) will not necessarily contain the same electrode materials as one designed for high energy (i.e., for an EV). As is shown in Fig. 2.1, power translates into acceleration, and energy into range, or miles traveled, for vehicular uses. Furthermore, performance, cost, and abuse-tolerance requirements for traction batteries [11] differ considerably from those for consumer electronics batteries. Vehicular applications are particularly sensitive to cost; currently, Li-ion batteries are priced at about US $1,000/kWh, whereas the USABC goal is US $150/kWh [12]. The three most expensive components of a Li-ion battery, no matter what the configuration, are the cathode, the separator, and the electrolyte [13]. Reduction of cost has been one of the primary driving forces for the investigation of new cathode materials to replace expensive $LiCoO_2$, particularly for vehicular applications. Another extremely important factor is safety under abuse conditions such as overcharge. This is particularly relevant for the large battery packs intended for vehicular uses, which are designed with multiple cells wired in series arrays. Premature failure of one cell in a string may cause others to go into overcharge during the passage of current. These considerations have led to the development of several different types of cathode materials, as will be covered in the next section. Because there is not yet one ideal material that can meet requirements for all applications, research into cathodes for Li-ion batteries is, as of this writing, a very active field.

Characteristics of Battery Cathode Materials

Modern cathode materials for Li-ion batteries are generally prepared in the lithiated (discharged) state, so that they can be paired with delithiated anodes such as graphite. For ease of handling, it is desirable that the material be reasonably air-stable at room temperature. Furthermore, graphite anodes impose a penalty of approximately 0.1 V in average cell potential compared to Li metal. To compensate for this, and also to maximize energy density, cathodes intended for use in Li-ion batteries have higher average potentials versus Li/Li^+ than earlier materials such as TiS_2 and vanadates [14] developed for Li metal batteries. Furthermore, the requirement for high specific capacity generally restricts choices to compounds containing first-row transition metals (usually Mn, Fe, Co, and Ni). Environmental and toxicity concerns have precluded the development of most V or Cr-containing materials, although electroactive compounds containing these metals exist. Today's technologically important cathodes fall into two broad categories: metal oxides and polyanionic compounds.

Figure 2.2 shows representations of the crystal structures of the most commonly used cathode materials for Li-ion batteries, and Table 2.1 summarizes their general properties. Figure 2.3 shows typical discharge profiles of selected materials in Li half-cell configurations.

Layered Transition Metal Oxides

$LiCoO_2$ was the first of the layered transition metal oxides to be commercialized, and is still used today in batteries for consumer devices. It has the structure shown in Fig. 2.2a, where Co and Li, located in octahedral sites, occupy alternating layers

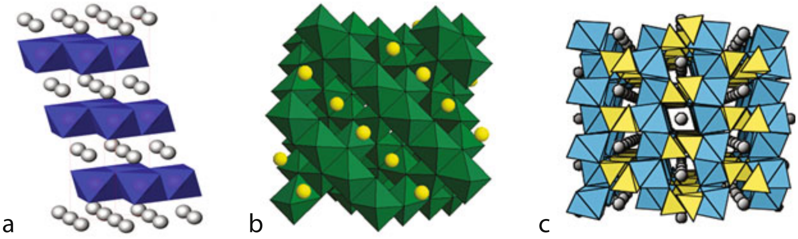

Fig. 2.2 Structures of common cathode materials: (**a**) The layered structure of $LiCoO_2$ with *c*-axis oriented vertically. The octahedrally coordinated Li ions in *3a* sites are represented as spheres and CoO_6 (Co in *3b* sites) as octahedra; (**b**) the cubic structure of $LiMn_2O_4$ spinel, with tetrahedrally coordinated Li ions (in *8a* sites) represented as spheres, and MnO_6 (Mn in *16d* sites) as octahedra; and (**c**) the olivine structure of $LiFePO_4$, looking down the *b*-axis. Octahedrally coordinated Li ions are represented as spheres, and FeO_6 and PO_4 as octahedra and tetrahedra, respectively

Table 2.1 Characteristics of commercial Li-ion battery cathode materials

Material	Structure	Potential versus Li/Li^+, average V	Specific capacity, mAh/g	Specific energy, Wh/kg
$LiCoO_2$	Layered	3.9	140	546
$LiNi_{0.8}Co_{0.15}Al_{0.05}O_2$ (NCA)	Layered	3.8	180–200	680–760
$LiNi_{1/3}Co_{1/3}Mn_{1/3}O_2$ (NMC)	Layered	3.8	160–170	610–650
$LiMn_2O_4$ and variants (LMO)	Spinel	4.1	100–120	410–492
$LiFePO_4$ (LFP)	Olivine	3.45	150–170	518–587

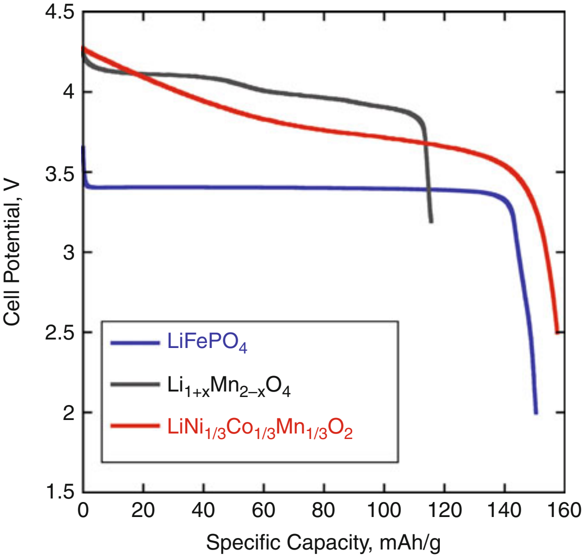

Fig. 2.3 Discharge profiles of lithium cells containing $LiFePO_4$, $Li_{1+x}Mn_{2-x}O_4$, or $LiNi_{1/3}Co_{1/3}Mn_{1/3}O_2$ electrodes

along the 111 planes in a cubic close-packed (ccp) oxygen array, to form a structure with overall hexagonal symmetry (space group R-3m). This type of stacking arrangement is called O3 in layer notation, indicating that there are three transition metal layers per unit cell and the Li ions are octahedrally coordinated.

Delithiation proceeds topotactically [15, 16] and is reversible over the composition range $1 \geq x \geq \sim 0.5$ for x in Li_xCoO_2, giving a practical specific capacity of about 140 mAh/g below 4.2 V versus Li/Li^+. Extraction of lithium to values of $x < \sim 0.5$ results in higher practical capacities initially, but often increases cycling losses [17]. This has been attributed to side reactions involving particle surfaces, which increase cell impedance, and to structural instability associated with phase changes at very low values of x in Li_xCoO_2 [18–21]. Coating $LiCoO_2$ particles, or rigorous heat treatment to remove surface species [22–24], results in improved cycling below 4.5 V versus Li/Li^+, but full delithiation is still not possible without cycling losses.

A layered compound with the nominal composition of $LiNiO_2$ has also been extensively studied for battery applications [25–28]. Its lower cost compared to $LiCoO_2$, and the potential for higher energy density were driving forces for its development. Although the structure is similar to $LiCoO_2$, $LiNiO_2$ readily exhibits non-stoichiometry. During synthesis, there is a tendency toward loss of lithium and reduction of some Ni to the +2 oxidation state. The Ni^{2+} migrates to Li^+ *3a* sites, due to the similarities in size between the two types of ions. The actual composition can be written as $Li_{1-z}Ni_{1+z}O_2$ with $0 < z < 0.2$, or as $(Li_{1-z}Ni_z{}^{2+})_{3a}(Ni_z{}^{2+}Ni_{1-z}{}^{3+})_{3b}O_2$ [29]. The degree of disorder is influenced by the synthetic conditions, and the electrochemical properties (e.g., the first cycle reversibility) are affected by the degree of non-stoichiometry [30, 31]. The difficulty in synthesizing high-quality $LiNiO_2$ was one impediment to its widespread adoption as a cathode material in Li-ion batteries, although nearly ideal structures can be obtained if sufficient care is taken [29]. (However, perfectly stoichiometric $LiNiO_2$ materials probably do not exist). Partial substitution of Ni with Co [32] was later found to be effective at reducing the cationic disorder on *3a* sites, leading to compositions such as $LiNi_{0.8}Co_{0.2}O_2$. Cobalt also helps to reduce oxygen loss at high states-of-charge, improving safety.

The thermal instability of Li_xNiO_2 at high states-of-charge [33–36] also raised a great deal of concern about the safety of this material when used as a cathode. The properties of $LiNiO_2$ have been improved via coating and doping with Mg, leading to a very high-capacity electrode material [37] with better thermal properties. However, the most commonly used electrode material related to $LiNiO_2$ is $LiNi_{0.8}Co_{0.15}Al_{0.05}O_2$ or NCA, which is now commercially produced (see Table 2.1 for general properties). The presence of Al in NCA improves both the thermal [33–36] and electrochemical properties [38, 39]. The high specific capacity and good power capability of this material make it attractive for vehicular applications although it is still not considered as inherently safe as other candidates such as LFP (see Table 2.2 and the discussion of olivines below).

Several ternary Li-Fe-O phases exist with differing arrangements of cations in cubic close-packed oxygen arrays [40]. However, $LiFeO_2$ with the R-3m structure

Table 2.2 Relative merits of selected commercial Li-ion battery cathodes

Advantages	Disadvantages
LMO ($LiMn_2O_4$ and variants)	
Low cost	Mn solubility issue, affecting cycle life
Excellent high rate performance	Low capacity
High operating voltage	
No resource limitations	
Moderate safety (oxygen release)	
LFP ($LiFePO_4$ and variants)	
Moderately low cost	Low operating voltage
Excellent high rate performance	Low capacity, especially for substituted variants
No resource limitations	Controlling patents
Very slow reaction with electrolyte	
Excellent safety (no oxygen release)	
NMC ($LiNi_{1/3}Co_{1/3}Mn_{1/3}O_2$) and variants	
High capacity	High cost of Ni and Co
High operating voltage	Potential resource limitations
Slow reaction with electrolytes	Relatively new in performance
Moderate safety (oxygen release)	Controlling patents
NCA ($LiNi_{0.8}Co_{0.15}Al_{0.05}O_2$)	
Performance is well established	High cost of Ni and Co
Slow reaction with electrolytes	Potential resource limitations
High capacity	Controlling saft patents
High voltage	
Excellent high rate performance	

is metastable and generally must be prepared via indirect methods such as ion exchange of $NaFeO_2$. The electrochemical properties of this material [41] and most other polymorphs [42, 43] are not, however, suitable for lithium-ion batteries due to low and highly sloping voltage profiles or poor cycling properties. Li_5FeO_4 with the anti-fluorite structure has a potential profile that may be compatible in a Li-ion battery configuration, but delithiation does not appear to proceed via simple oxidative deintercalation [44]. This material has been proposed for use as a lithium-ion source for lithium-ion batteries (i.e., to lithiate graphite anodes so that cathodes in the charged state may be used).

Ternary Li-Mn-O phases with Mn in the +3 or +4 oxidation state crystallize as spinels, the rock salt structure Li_2MnO_3, or as orthorhombic $LiMnO_2$ with a corrugated structure (o-$LiMnO_2$) but not as O3 layered structures. Lithium manganese oxide spinels (LMO) are technologically important cathodes and will be considered in a later section (*vide infra*). The Na-Mn-O system contains numerous polymorphs, including layered structures. $NaMnO_2$ has the same stacking arrangement as $LiCoO_2$, but is monoclinically distorted (space group C2/m), due to the abundance of Jahn–Teller distorted Mn^{3+} ions. Ion exchange of this compound yields a layered $LiMnO_2$ (designated O'3, with the prime indicating the monoclinic distortion) [45], but it rapidly converts to spinel upon electrochemical cycling, as does orthorhombic $LiMnO_2$ [46]. O'3-$LiMnO_2$, o-$LiMnO_2$, and spinel manganese oxide all have cubic close-packed oxygen arrays and differ only in the cation arrangement. Upon electrochemical delithiation of the first two materials, disproportion of Mn^{3+} into Mn^{2+} and Mn^{4+} ions occurs and Mn^{2+} ions subsequently migrate into vacant sites in the lithium layers via low-energy pathways, facilitating structural rearrangement to spinel [47].

Lithium-deficient layered Li_xMnO_{2+y} ($x \approx 0.7$, $y \geq 0.05$), which has an O2 rather than O3 stacking arrangement, does not convert to spinel upon cycling [48, 49], because the oxygen array is not ccp. In addition, non-stoichiometric lithium manganese oxides that are intergrowths of O2 and O3 phases show better resistance to conversion than the pure O3 structure [50, 51]. The presence of transition metal vacancies in these compounds (which reduce the concentration of the Jahn–Teller Mn^{3+} ions) results in low rate capability, because the vacancies tend to trap nearby lithium ions, impeding their mobility [52].

Other lithium manganese oxides with tunnel structures [53–55] exhibit interesting electrochemical properties, particularly those based on the $Na_{0.44}MnO_2$ structure. This material has excellent cycling characteristics [56] and rate capability [57], and does not convert to spinel, although the practical capacity is limited by voltage considerations (the average potential at which lithium is extracted is the highest of any known manganese oxide [58]). All of these tunnel and O2 or O2/O3 layered materials, however, must be prepared via ion exchange of their sodium manganese oxide structural analogs, complicating their preparation. Furthermore, the lithium deficiency of the ion-exchanged materials limits the capacity in Li-ion battery configurations, as all of the cycleable lithium must originate from the cathode.

Li_2MnO_3 can be considered a layered structure similar to $LiCoO_2$, but with 111 planes alternately occupied by Li and $Li_{1/3}Mn_{2/3}$. Ordering of Li and Mn in the transition metal layer imposes a monoclinic superstructure, but the stacking arrangement is essentially identical to that of the R-3m structures discussed above. Mn in this compound is tetravalent and all lithium sites are occupied, precluding either oxidative deintercalation or reductive intercalation. Nevertheless, several researchers have observed electrochemical activity of Li_2MnO_3 when it is charged in lithium half-cells to high potentials [59]. Recent evidence [60] suggests that lithium deintercalation occurs with simultaneous oxygen loss during the initial charge, as well as H^+/Li^+ exchange. The converted material becomes electroactive and can subsequently be lithiated during cell discharge. Acid leaching of Li_2MnO_3 also yields an electroactive manganese oxide phase [61]. The reaction involves loss of Li_2O from the structure and ion exchange, to produce layered $H_{1-x}Li_x[Li_{0.33}Mn_{0.67}]O_2$ [62].

The compound $Li_{1.2}Mn_{0.4}Cr_{0.4}O_2$ [63] is essentially a solid solution of layered Li_2MnO_3 and $LiCrO_2$ with an O3 stacking arrangement [64]. Very high discharge capacities (~200 mAh/g) can be obtained based on $Cr^{3+} \leftrightarrow Cr^{6+}$ redox processes. Conversion to spinel phases does not occur because Mn remains in the +4 oxidation state throughout charge and discharge, nor does the electrode need chemical or electrochemical activation prior to use. Nevertheless, concerns over the environmental impact of hexavalent chromium have prevented further development of this material.

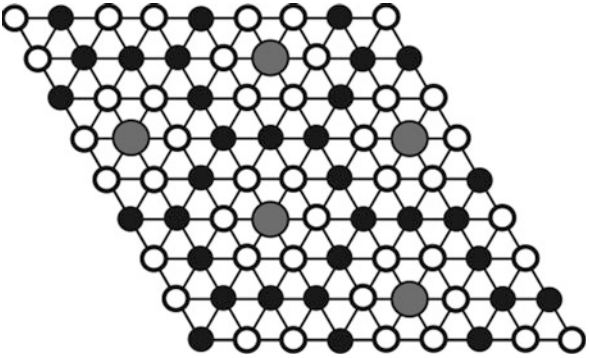

Fig. 2.4 A transition metal layer in $LiNi_{0.5}Mn_{0.5}O_2$ showing the flower pattern. Li is represented by the large gray circles, Mn by small white circles, and Ni by black circles (Used with permission from Ref. [71])

The search for improved layered oxide materials containing low-cost transition metals ultimately led to the discovery of $LiNi_{0.5}Mn_{0.5}O_2$ [65–67] as well as compounds with the general composition $Li[Ni_xLi_{(1/3-2x/3)}Mn_{(2/3-x/3)}]O_2$ [68]. Computational modeling [69] and spectroscopic investigations [70] show that the Ni and Mn in these materials are in the +2 and +4 oxidation states, respectively. During normal charge processes in an electrochemical cell, nickel is ultimately oxidized to the +4 oxidation state, and Mn remains tetravalent. $LiNi_{0.5}Mn_{0.5}O_2$ does not convert to spinel upon cycling, unlike the metastable O3-$LiMnO_2$, because no trivalent Mn is ever produced in the structure.

The defect chemistry of $LiNi_{0.5}Mn_{0.5}O_2$ also distinguishes it from $LiNiO_2$ (where nickel is primarily in the +3 oxidation state initially) discussed above. A feature of $LiNi_{0.5}Mn_{0.5}O_2$ is anti-site mixing [65–67, 71, 72] in which some Ni^{2+} ions are located on the Li *3a* sites, and some Li^+ ions on transition metal *3b* sites, that is, $(Li_{1-x}Ni_x)_{3a}(Li_xNi_{0.5-x}Mn_{0.5})_{3b}O_2$, $x \approx 0.08-0.12$. Mn ions in the transition metal layers preferentially surround the Li ions located in 3*a* sites to form Li_2MnO_3-like clusters, and Ni ions occupy sites adjacent to Mn, to form a “flower pattern” (Fig. 2.4). The anti-site mixing is thought to be a thermodynamically favored feature of the ion ordering and thus intrinsic to the structure. Unlike with $LiNiO_2$, simple manipulation of conditions during direct synthesis is therefore not likely to result in a near-ideal layered structure.

$Li[Ni_xLi_{(1/3-2x/3)}Mn_{(2/3-x/3)}]O_2$ compounds can be considered solid solutions of Li_2MnO_3 and $LiNi_{0.5}Mn_{0.5}O_2$. Although the discharge capacity between 4.4 and 3.0 V versus Li/Li^+ drops as the Ni content decreases, the opposite trend is observed after cell charge to 4.8 V and subsequent discharge to 2.0 V [73]. In addition, the Li_2MnO_3-rich materials exhibit a plateau at about 4.5 V during charge, the length of which is inversely proportional to x. This is thought to be deintercalation of Li ions with concomitant loss of oxygen (for a net loss of Li_2O), similar to what happens when Li_2MnO_3 is charged in an electrochemical cell. This process can result in very high discharge capacities upon subsequent cycles (e.g., 230 mAh/g for $x = 1/3$).

An advantage to these materials and related Li-rich materials (where excess lithium replaces some of the transition metal ions on *3b* sites, but the Mn content still equals that of the Ni content) is decreased cation mixing. This improves rate capability [74] as compared to $LiNi_{0.5}Mn_{0.5}O_2$.

The presence of a relatively large number of Ni ions in the Li *3a* sites of the $LiNi_{0.5}Mn_{0.5}O_2$ structure due to the anti-site mixing has a negative impact on the Li diffusivity, resulting in a low-rate cathode material. $LiNi_{0.5}Mn_{0.5}O_2$, prepared by low-temperature ion exchange of the nearly perfectly layered $NaNi_{0.5}Mn_{0.5}O_2$ analog, is capable of sustaining higher discharge currents than samples prepared by conventional methods [75]. However, the most successful method used to address this issue has been to incorporate some cobalt into the structure [76]. The best known of these compounds is $Li[Ni_{1/3}Co_{1/3}Mn_{1/3}]O_2$, sometimes referred to as NMC (Tables 2.1 and 2.2). This compound is gradually replacing $LiCoO_2$ in consumer batteries (in some cases, a mixture of the two are used as the cathode) and is under consideration for some vehicular applications. The voltage profile of NMC versus Li/Li^+ is gradually sloping (Fig. 2.3), as is typical of many layered compounds, and provides a somewhat higher capacity than $LiCoO_2$ below 4.3 V versus Li/Li^+ (typically about 160 mAh/g compared to 140). Capacities in excess of 200 mAh/g can be achieved when cells are charged to higher voltage limits, although this usually results in diminished cycle life.

The oxidation states of Ni, Co, and Mn in as-made $Li[Ni_{1/3}Co_{1/3}Mn_{1/3}]O_2$ are +2, +3, and +4, respectively [77]. First principle calculations suggest that Ni^{2+} is ultimately oxidized to Ni^{4+} during extraction of the first two-thirds of the lithium during electrochemical charging in lithium cells, and oxidation of Co^{3+} to Co^{4+} occurs only during removal of the last one-third [78] (i.e., at high cell potentials). As in $LiNi_{0.5}Mn_{0.5}O_2$, Mn remains inactive throughout normal operating cell voltages. The redox activity of Ni during the extraction of lithium from $Li[Ni_{1/3}Co_{1/3}Mn_{1/3}]O_2$ has been verified by in situ X-ray absorption spectroscopic (XAS) studies, although the details of the participation of Co in the electrochemistry are less clear [79–83]. Charge compensation associated with Co is currently thought to occur, at least partially, at oxygen sites, due to the covalency of the Co-O bonds.

The improved electrochemical properties and better structural, chemical, and thermal stability [84, 85] of $Li[Ni_{1/3}Co_{1/3}Mn_{1/3}]O_2$ compared to $LiCoO_2$ or NCA render it an attractive replacement cathode material for consumer batteries. Nevertheless, the presence of a significant amount of costly cobalt, albeit in reduced quantities compared to $LiCoO_2$, may still make it too expensive for most vehicular applications. Compounds having the general formula $Li[Ni_xCo_{1-2x}Mn_x]O_2$ with $x = 0.4$ or 0.45 have recently been developed by Whittingham and coworkers specifically to address the cost issue [86–89]. Although the amount of anti-site mixing increases with larger x, these materials exhibit very good electrochemical performances. The effect of increasing the Ni content of these materials on the thermal stability, especially at high states of charge, remains to be determined, however.

Another approach has been to partially substitute another metal such as aluminum for cobalt [89, 90]. Although the amount of substitution must be kept low to maintain the high specific capacities, both the thermal stability of the delithiated materials [91] and the electrochemical properties [92, 93] appear to be enhanced.

All of the NMCs discussed above contain equal amounts of Ni and Mn, which ensure that the oxidation states of the two metals are primarily +2 and +4, respectively. Recent attempts to increase Mn content in stoichiometric materials having the formula $Li[Ni_{0.45-x}Co_{0.1}Mn_{0.45+x}]O_2$ yielded phase mixtures for values of $x > 0.05$ [94] and a solid solution phase for $x = 0.05$. In this compound, $Li[Ni_{0.4}Co_{0.1}Mn_{0.5}]O_2$, the extra manganese is in the +3 oxidation state. Unfortunately, this material exhibits poorer capacity retention upon electrochemical cycling and lower rate capability than $Li[Ni_{0.45}Co_{0.1}Mn_{0.45}]O_2$. It is, however, possible to form solid solutions between $Li[Ni_{1/3}Co_{1/3}Mn_{1/3}]O_2$ and Li_2MnO_3 to make Li- and Mn-rich materials where the excess Mn is in the +4 oxidation state. As with the related $Li[Ni_xLi_{(1/3-2x/3)}\ Mn_{(2/3-x/3)}]O_2$ compounds, these materials can be electrochemically activated during charge to high potentials in lithium cells. The activation process (deintercalation of Li, concomitant loss of oxygen, and H^+/Li^+ ion exchange) yields electrodes with discharge capacities as high as 290 mAh/g [95, 96]. The very high capacities make these materials interesting for both consumer and automotive applications, and they are now being actively developed (e.g., by Envia Systems, Newark, CA).

Manganese Oxide Spinels

The marked tendency for many manganese oxide phases to convert to spinel structures during lithiation in electrochemical cells, or upon heating with a lithium source, attests to the stability of this structure in the Li-Mn-O system. The stoichiometric spinel, $LiMn_2O_4$, is easily synthesized in air from a variety of Li and Mn-containing precursors. Figure 2.2b shows its cubic structure (space group Fd-3m), where Li ions occupy tetrahedral *8a* sites and Mn is located in octahedral *16d* sites in a ccp array of oxygen anions. In addition, there are vacant tetrahedral and octahedral interstitial sites in the three-dimensional structure that provide pathways for lithium diffusion.

Early work [97] showed that it is possible to remove lithium from $LiMn_2O_4$ using a mild acid treatment. During this process, Mn is oxidized from an average +3.5 oxidation state to +4, and λ-MnO_2, which retains the spinel framework, is formed (Eq. 2.1). In addition, some dissolution of Mn occurs:

$$2LiMn_2O_4 + 4H^+(aq) \rightarrow 2Li^+(aq) + Mn^{2+}(aq) + 2H_2O + 3\,\lambda\text{-}MnO_2 \qquad (2.1)$$

Oxidative extraction of lithium from the tetrahedral *8a* sites of $LiMn_2O_4$ to form λ-MnO_2 in a lithium cell [98, 99] was subsequently demonstrated to occur slightly above 4 V. It is also possible to insert lithium into the vacant octahedral sites of

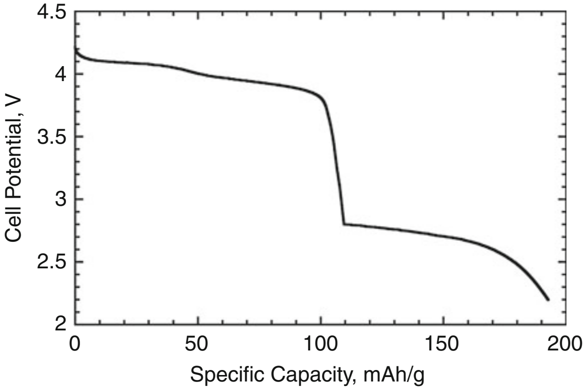

Fig. 2.5 Discharge profile of a Li/modified-$LiMn_2O_4$ cell at 0.1 mA/cm^2. Cell was initially discharged to 2 V and then charged to 4.3 V. This was the third discharge between 4.3 and 2.0 V

$LiMn_2O_4$ either chemically or electrochemically, with concomitant reduction of Mn. When carried out in a cell with a lithium anode, this process occurs below 3 V, and the discharge profile is flat, indicative of a two-phase reaction. The tetragonally distorted phase $Li_2Mn_2O_4$ (space group $I4_1/amd$) is formed due to the cooperative Jahn–Teller effect, which occurs when more than half the manganese is in the form of d^4 Jahn–Teller Mn^{3+} ions. The phase transition results in a 16% increase in the c/a ratio [100] ($a = c = 8.248$ Å in $LiMn_2O_4$; $a = 8.007$ Å, $c = 9.274$ Å in $Li_2Mn_2O_4$). In theory, lithium cells containing $LiMn_2O_4$ can either be charged or discharged initially, and then cycled over a composition range of $0 \leq x \leq 2$ in $Li_xMn_2O_4$ to give a total specific capacity of 285 mAh/g. Figure 2.5 shows the voltage profile of a Li/modified $LiMn_2O_4$ cell assembled in the author's laboratory, after discharging into the 3 V region and full recharge. Both 4 and 3 V plateaus are evident; although the overall capacity is somewhat lower than the theoretical value.

The large anisotropic volume change associated with formation of tetragonal $Li_2Mn_2O_4$ results in particle disintegration and loss of connection within the composite electrode. This causes such a rapid loss of capacity that, in practice, the cycle lives of cells containing $LiMn_2O_4$ discharged even a few times into the 3 V region are greatly compromised. In contrast, the extraction of lithium from $LiMn_2O_4$ above 4 V versus Li/Li^+ maintains the cubic structure and results in smaller volume changes. For this reason, discharge is typically limited to the 4 V plateau (Fig. 2.3), which exhibits much better reversibility. The theoretical capacity associated with this plateau is 148 mAh/g, although it is difficult to fully extract all the lithium, resulting in somewhat lower practical values.

From the early 1990s onward, intensive efforts were devoted to the development of $LiMn_2O_4$ for lithium-ion batteries, particularly at Bellcore Laboratories [101–103]. Although limiting discharges to the 4 V plateau resulted in much better cycling than when both the 3 and 4 V plateaus were utilized, gradual capacity fading was still observed [104]. This behavior was attributed to several factors, including irreversible side reactions with the electrolyte due to the high potential, loss of oxygen from the delithiated spinel, dissolution of Mn, and production

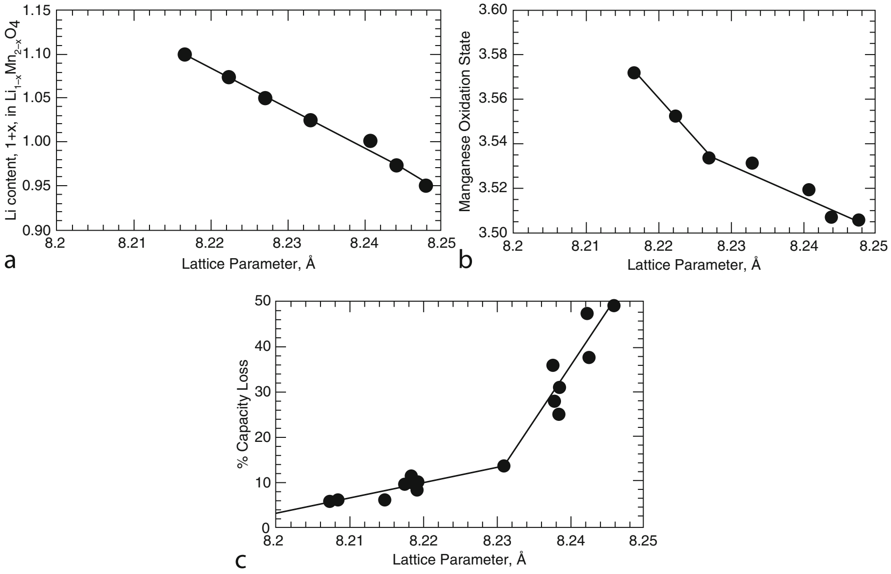

Fig. 2.6 (**a**) The variation of the lattice parameter, *a*, with the lithium content of $Li_{1+x}Mn_{2-x}O_4$; (**b**) the variation of lattice parameter with the average Mn oxidation state in $Li_{1+x}Mn_{2-x}O_4$; and (**c**) relationship between capacity loss after 120 cycles and the lattice parameter in $Li_{1+x}Mn_{2-x}O_4$ (Used with permission from Ref. [113])

of tetragonal $Li_2Mn_2O_4$ at particle surfaces, particularly at high discharge rates [100, 105].

Partial substitution of Mn to form $LiM_xMn_{2-x}O_4$ improves capacity retention [106–112]. Of particular interest are the lithium-substituted materials having the general formula $Li_{1+x}Mn_{2-x}O_4$. As lithium is substituted for manganese on the *16d* sites (x is increased), the average oxidation state of the latter rises. This effectively decreases the 4 V capacity in proportion to the amount of substitution but results in a higher average oxidation state of the Mn at the end-of-discharge. This ameliorates the tendency to form the tetragonally distorted phase under nonequilibrium conditions such as rapid discharging, because this occurs only when the Mn oxidation state falls below an average of 3.5. Because Mn is fully oxidized before all the lithium can be extracted from *8a* sites, side reactions are suppressed. Finally, dissolution of Mn decreases because this phenomenon is dependent on the concentration of trivalent ions.

Li substitution and the attendant increase in Mn oxidation state in the as-made $Li_{1+x}Mn_{2-x}O_4$ compounds decrease the lattice parameter, a (Fig. 2.6a and b). The magnitude of this value correlates closely with the amount of capacity loss upon cycling (Fig. 2.6c), so that it can be used to predict the cycling behavior of the spinel materials [113]. In particular, improvements are most marked when $a \leq 8.23$ Å. Because the cycling behavior is so much better than $LiMn_2O_4$, nearly all commercial manganese oxide spinel materials (LMOs) made today are lithium substituted. These have theoretical specific capacities of 100–120 mAh/g (Table 2.1), somewhat lower than that for $LiMn_2O_4$.

The maximum possible substitution in $Li_{1+x}Mn_{2-x}O_4$ corresponds to $x = 1/3$ (the compound $Li_{4/3}Mn_{5/3}O_4$ or $Li_4Mn_5O_{12}$), at which point all of the Mn is in the +4 oxidation state and there is no 4 V capacity, because oxidative extraction of lithium cannot occur. Nevertheless, it is possible to insert lithium reversibly into octahedral *16c* sites at about 2.9 V versus Li/Li^+ until a composition of $Li_7Mn_5O_{12}$ is reached, for a total of 156 mAh/g [114, 115]. The cubic symmetry is maintained until about $Li_{6.5}Mn_5O_{12}$, at which point Mn is reduced to an average oxidation state of 3.5 and the cooperative Jahn–Teller effect induces a tetragonal distortion. Because this process occurs only at the end-of-discharge, $Li_4Mn_5O_{12}$ exhibits much better cycling behavior on the 3 V plateau than does $LiMn_2O_4$. However, the low operating voltage and capacity, and the inability to extract lithium makes $Li_4Mn_5O_{12}$ impractical for Li-ion batteries.

It is also possible to prepare cation-deficient or defect spinels, $Li_{1-x}Mn_{2-2x}O_4$ [114]. The cation vacancies increase the average oxidation state of Mn and decrease the capacity above 4 V in favor of that below 3 V, proportionally with x. In the end-member compound $Li_2Mn_4O_9$ (corresponding to $x = 0.11$ in $Li_{1-x}Mn_{2-2x}O_4$), all Mn is tetravalent, and lithium cannot be extracted, so that there is no capacity at 4 V. Lithium can be inserted below 3 V versus Li/Li^+, to a maximum composition of $Li_5Mn_4O_9$. Although the theoretical capacity (213 mAh/g) is higher than that of $Li_4Mn_5O_{12}$, approximately 1/3 of it is associated with the formation of the Jahn–Teller distorted tetragonal phase.

In principle, defect spinels with values of $x < 0.11$ should cycle on the 4 V plateau better than $LiMn_2O_4$ for the same reasons as the lithium-rich stoichiometric spinels. In practice, it is difficult to control the degree of non-stoichiometry during synthesis, so these materials are not of interest commercially.

In spite of the improved performance exhibited by the lithium-substituted spinels, capacity fading upon cycling is still observed in electrochemical cells, particularly at elevated temperatures (55°C) [116–121]. This has negative implications particularly for vehicular applications, where batteries may be subjected to a wide variety of operating and storage conditions, including very warm environments. The dissolution is associated with Mn^{3+} disproportionation (Eq. 2) in the presence of acidic components of the $LiPF_6$/organic carbonate electrolyte solutions used in Li-ion batteries.

$$2Mn^{3+}(\text{solid}) \rightarrow Mn^{4+}(\text{solid}) + Mn^{2+}(\text{solution}) \qquad (2.2)$$

Loss of manganese leads to the formation of a defect spinel structure with reduced or no 4 V capacity [104, 116–121]. Additionally, proton exchange [116–121], phase separation, film formation, and precipitation of MnO and MnF_2 may occur, increasing cell impedance and exacerbating the capacity fading. More significantly, dissolved Mn^{2+} can cross over to the anode, become reduced, and precipitate as the metal, increasing the charge-transfer resistance and disrupting the critical SEI layer [122, 123]. The graphite anode is markedly more sensitive to this effect than lithium is. Thus, assessment of spinel cathodes to determine the effectiveness of an approach to improve resistance to dissolution should ultimately be carried out in a full cell configuration rather than in lithium half-cells.

Some methods designed to address the problem of spinel dissolution include coating of particles [124, 125] and the use of new non-fluorinated salts such as lithium bis(oxalato)borate (LiBOB) which do not generate HF in situ [126–128]. Interestingly, dissolution of manganese appears to be suppressed in electrodes where LMO is mixed with an NMC [129]. Although the cycling behavior of Li-ion cells with spinel electrodes is still inferior to that of devices containing alternative commercial cathode materials (Table 2.2), other aspects of performance such as rate capability and safety [33–36, 130], the wide availability of manganese precursors, and the potential for low cost make LMO attractive especially for vehicular applications. Thus, at least one battery manufacturer focused on vehicle technologies (e.g., Enerdel, Indianapolis, IN) is pursuing the development of Li-ion batteries with spinel cathodes and hard carbon anodes (which are less sensitive to the effects of manganese dissolution than graphite).

Several lithium-containing oxide spinels having transition metals other than Mn can also be synthesized. One example is $LiCo_2O_4$, which can be prepared from a low-temperature form of $LiCoO_2$ [131]. (The latter, known as LT-$LiCoO_2$, has a structure intermediate between that of a spinel and layered compound). Another is $LiNi_2O_4$ [25]. Unlike $LiMn_2O_4$, the electrochemical characteristics of most of these spinels are inferior to those of the layered analogs, so that they are not of technological interest as cathode materials. However, $Li_4Ti_5O_{12}$ (LTO), which, because of its voltage properties, functions as an anode material, demonstrates excellent cycling performance. Although the energy density is lower than that of graphite, it does not require the formation of an SEI. Thus, it is also an attractive match for LMO cathode materials. Batteries with LTO anodes and LMO or other high-voltage cathodes may find utility in HEVs, which do not require as high an energy density as pure EVs.

The intensive search for substituted lithium manganese spinels with better cycling performance led to the discovery of several materials having capacity near 5 V versus Li/Li^+. These include spinels substituted with Cr, Fe, Cu, Co, or Ni [132–136]. In most cases, these materials exhibit a plateau near 4 V as well as a second plateau near 5 V, with the magnitude of the latter increasing with larger x in $LiM_xMn_{2-x}O_4$ (where M = Cr, Fe, Cu, Co, or Ni). The 4 V capacity is associated with the usual Mn^{3+}/Mn^{4+} spinel redox couple, whereas the higher voltage plateau is associated with redox processes of the substituting metal. Interestingly, the compound $LiNi_{1/2}Mn_{3/2}O_4$ has very little 4 V capacity, unlike other $LiM_{1/2}Mn_{3/2}O_4$ spinels [137] (Fig. 2.7).

In the case of $LiNi_{1/2}Mn_{3/2}O_4$, nearly all of the Mn is tetravalent [136], so that further oxidation is not possible. The specific capacity of 147 mAh/g at 4.7 V is associated with Ni^{2+}/Ni^{4+} redox processes. The high energy density and high voltage makes this material attractive for vehicular applications, because fewer cells need to

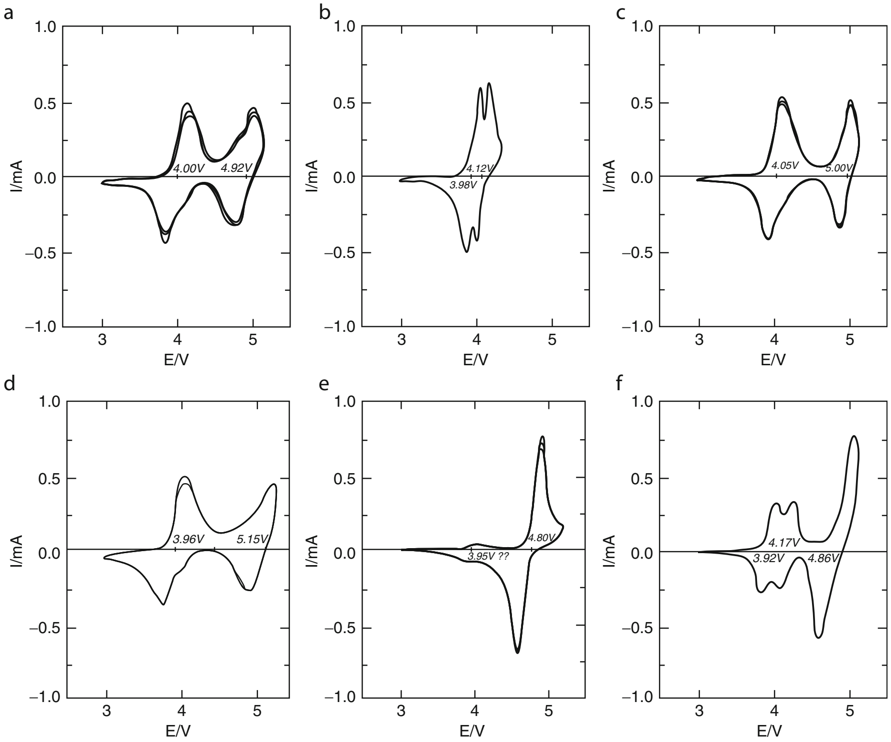

Fig. 2.7 Slow-scan voltammetry of Li/LiM$_{1/2}$Mn$_{3/2}$O$_4$ cells with M = (**a**) Cr, (**b**) Mn, (**c**) Fe, (**d**) Co, (**e**) Ni, and (**f**) Cu at a rate of 0.2 mV/s using 1 M LiPF$_6$ in 1:1 v/v EC/DEC electrolyte (Used with permission from Ref. [137])

be connected in series to make the 300 V packs used in electric vehicles. This simplifies engineering, results in comparatively higher energy density on the system level because less hardware is required, and lowers costs. ETV Motors of Herzliya, Israel, is one company actively developing LiNi$_{1/2}$Mn$_{3/2}$O$_4$ batteries for this purpose.

The very high potential at which this cathode operates, however, presents considerable challenges for cycle life. Although conventional carbonate-based electrolytes used in Li-ion batteries have, in principle, excellent oxidative stability, the presence of impurities such as water may contribute to side reactions that decrease resistance to irreversible oxidation, resulting in shortened battery lifetimes. In addition, cell components such as carbon additives used to improve conductivity in composite cathodes, or surfactants that aid in wetting may oxidize irreversibly at high potentials, and current collectors may corrode. Thus, cycling is usually restricted to a voltage range below about 4.3 V versus Li/Li$^+$ (4.2 V in cells with graphite anodes). Stringent purification of electrolytes and the use of special protective additives are allowing gradual extension of this range. In addition, the development of new electrolytes containing ionic liquids or sulfolanes is expected to enable high-voltage cell operation, although the choice of anode may then be restricted to LTO or other materials that do not require SEI formation. Other strategies to prolong the cycle life of cells containing $LiNi_{1/2}Mn_{3/2}O_4$ include treating active material particles with protective coatings to minimize direct contact with electrolyte solutions [138–140], or partial substitution of Ni or Mn with other cations such as Ti, Mg, or Zn [141–143].

Synthesis of $LiNi_{1/2}Mn_{3/2}O_4$ is normally carried out at high temperatures to ensure good crystallinity and to lower the surface area and thus minimize reactivity with electrolyte solutions and other components. Under these conditions, oxygen loss may occur, leading to the formation of a non-stoichiometric material ($LiNi_{1/2}Mn_{3/2}O_{4-x}$) containing some Mn^{3+} in the structure. Additionally, a rock salt impurity, $Li_xNi_{1-x}O$, is also produced. Annealing at 700°C partially reverses the oxygen loss, but the telltale 4 V capacity indicative of the presence of electroactive Mn^{3+} can often be observed in cells made with these materials (e.g., in Fig. 2.7e). Substitution with other metals, as discussed in the papers listed in Refs. [141–143], often decreases the amount of Mn^{3+} in these compounds, which may play a role in the observed improvements in cycling.

If the sample is cooled slowly during synthesis, an ordered phase can be produced (space group $P4_332$ with Ni in *4b* sites and Mn in *12d* sites [144]). The electrochemical properties (in particular, rate capability) of the ordered phase are inferior to those of the disordered non-stoichiometric phase [145, 146]. The mixed Mn valency in the disordered Fd-3m phase leads to an increase in the electronic conductivity of about 1.5 orders of magnitude compared to that of the ordered material. This is thought to be responsible for the increased rate capability of the former compared to the latter.

The presence of electroactive Mn in disordered $LiNi_{1/2}Mn_{3/2}O_4$ suggests that dissolution may be problematic, as it is with the $LiMn_2O_4$ variants. In spite of this and the high operating voltages, extremely stable cycling has been observed in full cell configurations, albeit with $Li_4Ti_5O_{12}$ anodes [147].

LiFePO₄ and Other Phospho-olivines

In 1997, Goodenough and coworkers reported on the electrochemical properties of a new class of cathode materials known as the phospho-olivines [148], which adopt the orthorhombic structure (space group Pnma) shown in Fig. 2.2c. In the case of $LiFePO_4$ (triphylite), Li^+ and Fe^{2+} occupy octahedral sites, and P is located in tetrahedral sites in a somewhat distorted hexagonal close-packed (hcp) oxygen array. The FeO_6 octahedra share corners and LiO_6 octahedra share edges along tunnels down the *b*-axis, through which the Li ions can diffuse. Extraction and reinsertion of Li from $LiFePO_4$ proceeds at about 3.45 V in a lithium cell with a theoretical specific capacity of 170 mAh/g. The potential is independent of the composition x in Li_xFePO_4 (i.e., the voltage profile is flat, Fig. 2.3) indicating that a two-phase reaction occurs. In situ X-ray diffraction and Mossbauer experiments

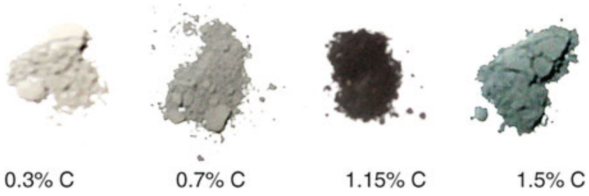

Fig. 2.8 Photographs of $LiFePO_4$ samples containing varying amounts of carbon (Used with permission from Ref. [153])

on Li/$LiFePO_4$ cells [149] show that the two relevant phases are triphylite and $FePO_4$, also known as heterosite (Eq. 2.3).

$$LiFePO_4\ (\text{triphylite}) \leftrightarrow FePO_4\ (\text{heterosite}) + e^- + Li^+ \tag{2.3}$$

Initial reports on the electrochemical characteristics of $LiFePO_4$ emphasized its poor rate capability and the lower than expected utilization in lithium cells even when discharged at low current densities (e.g., only about 60% in Ref. [149]). This was attributed to the low electronic conductivities of both the triphylite and heterosite phases [150]. Coating particles with carbon ameliorates the low conductivity and result in better rate performance [151]. This is most conveniently achieved by including a carbon source during initial synthesis of the $LiFePO_4$ sample. The presence of carbon or carbon-containing precursors during calcination in an inert atmosphere has several additional beneficial effects; it retards grain growth, resulting in small particles that allow rapid extraction of Li ions, and prevents formation of Fe^{3+}-containing impurities. It also allows the use of easy-to-handle, low-cost, Fe^{3+}-containing starting materials such as iron nitrate, which are reduced during the heating process [152].

In practice, many lab-synthesized samples of $LiFePO_4$ contain carbon, due to the use of precursors such as iron oxalate [153]. Even small amounts of carbon can result in drastic sample color changes from the off-white of native $LiFePO_4$ (Fig. 2.8). The electrochemical performance is also greatly affected by the carbon content, although this also depends on the distribution of carbon over particle surfaces and details of its structure [154–157]. Carbons produced in situ during synthesis of $LiFePO_4$ are disordered due to the relatively low calcination temperatures (generally, 600–700°C). Disordered carbons are less conductive than graphite, and conductivity depends on the size and number of graphene domains. The use of graphitization catalysts (often containing iron) improves the conductivity of coatings by several orders of magnitude, and can also result in co-production of carbon nanotubes or fibers, which wire particles together [158, 159]. The result is that very small amounts of carbon, often less than 2 wt.%, are sufficient to produce high-rate $LiFePO_4$ samples. This is important because too much lightweight carbon adversely affects the tap densities of $LiFePO_4$ composites, further decreasing the already somewhat low energy density [160].

The changes in sample color, increases in bulk conductivities, and improved electrochemical performance induced by the presence of very small amounts of carbon (or other highly colored impurities) complicate the interpretation of results of doping experiments intended to increase the intrinsic conductivity of $LiFePO_4$. A color change from off-white to black or gray should not be regarded as proof-positive of successful doping and increased intrinsic electronic conductivity, for the reasons described above. Even when carbonaceous precursors are not used, the use of organic solvents or plastic containers during grinding or other processing steps may introduce carbon. Early claims of successful low-level aliovalent substitution [161] on the Li sites of $LiFePO_4$, resulting in greatly enhanced conductivities and electrochemical performance, may have been a fortuitous consequence of well-distributed electronically conductive impurities such as carbon and metal-rich phosphides [162–166]. Recent studies of the defect chemistry of $LiFePO_4$ show that substitution of multivalent ions on the Li site is very limited, and always accompanied by lithium vacancies, so that no mixed valency for iron occurs [167]. Earlier computational modeling of the defect, dopant, and Li transport properties of $LiFePO_4$ [168] indicates that substitution of multivalent ions on Li or Fe sites (other than divalent ions on the latter) is not energetically favored. It was predicted that the most likely type of defect is the Li-Fe anti-site pair, in which Li^+ ions are located on Fe^{2+} sites and are balanced by an equal number of Fe^{2+} ions on Li sites. Recent work, however, shows that there is a marked asymmetry between the number of Fe ions on Li sites and vice versa [169–171]. Very few lithium atoms can be accommodated on iron sites. More commonly, Fe ions on Li sites are accompanied by a small number of vacancies, to form $[Li_{1-2x}Fe_x]FePO_4$. The presence of relatively immobile multivalent ions on Li sites interferes with fast Li diffusion, since $LiFePO_4$ is essentially a one-dimensional ion conductor [172–174]. Likewise, a large number of anti-site defects are likely to impact electrochemical performance adversely [175, 176] as is seen in Refs. [169–171]. At any rate, it is apparent that near room temperature, only a relatively small concentration of vacancies or interstitial defects is possible.

Carbon coatings, although convenient for the reasons stated above, are not absolutely necessary to assure good electrochemical performance [177], as long as particle sizes are kept small and particle size distributions are narrow. Nanostructuring reduces diffusion distances and ameliorates the effects of low electronic conductivity, allowing full discharge at even moderate to high rates. Subtle changes in the discharge characteristics of $LiFePO_4$ samples occur as particle size is decreased, most notably, a stronger dependence of voltage upon composition (x in Li_xFePO_4) close to the end-of-charge and end-of-discharge, implying solid-solution behavior [178, 179]. Other researchers have observed XRD, neutron diffraction, and electrochemical evidence of a small degree of lithium non-stoichiometry in larger Li_xFePO_4 particles at both composition extremes [180, 181], as illustrated in Fig. 2.9.

The existence of a small degree of non-stoichiometry (and thus mixed valence states for iron) may explain why this system is electroactive, given that both end members have such poor electronic conductivity. It should be noted, however, that kinetic effects, surface impurities, and the presence of defects [179, 182–184] also influence the shape of the Li/$LiFePO_4$ discharge profile. This makes it hard to

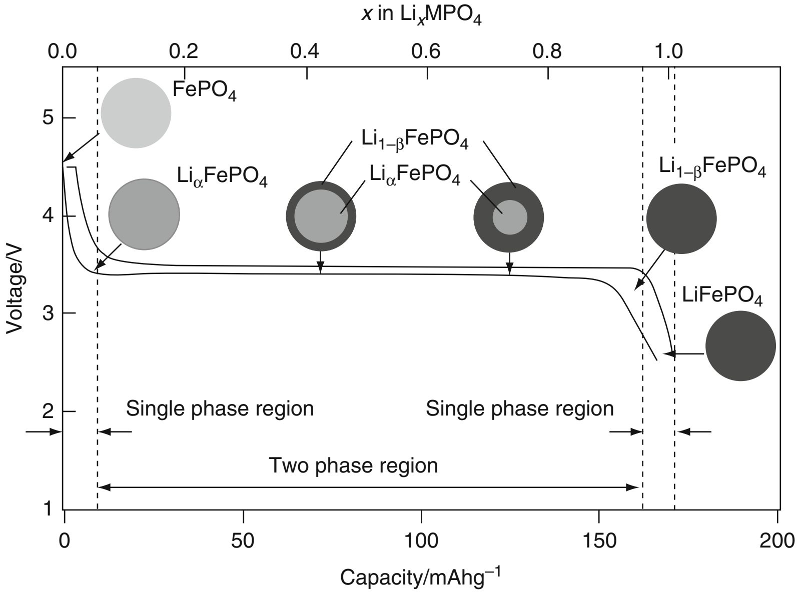

Fig. 2.9 Scheme of the discharge processes of Li$_x$FePO$_4$, showing solid-solution behavior close to $x = 0$ and $x = 1$ (Used with permission from Ref. [180])

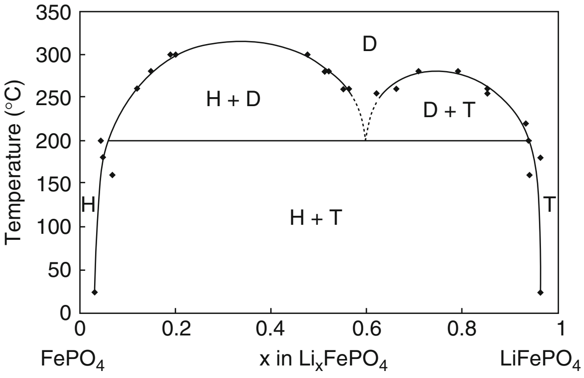

Fig. 2.10 Phase diagram of the Li$_x$PO$_4$ system, where T, H, and D denote triphylite, heterosite, and disordered (but not amorphous) phases, respectively (Used with permission from Ref. [186])

determine what the exact compositional ranges of solid-solution behavior are at room temperature from the electrochemical data alone. Complications from the effects of strain also make the interpretation of diffraction data difficult.

Experiments conducted on heated LiFePO$_4$/FePO$_4$ mixtures of varying concentrations [185, 186] show that solid solutions form from $0 \leq x \leq 1$ in Li$_x$FePO$_4$ at elevated temperatures, however. A representative phase diagram is shown in Fig. 2.10. The solubility limits of lithium in heterosite and vacancies in

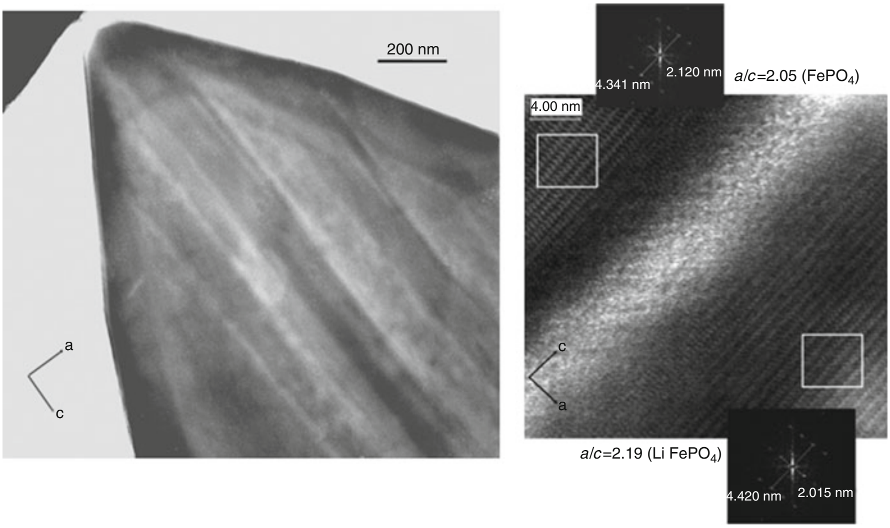

Fig. 2.11 *Left*: TEM image showing a partially delithiated crystal with the global composition $Li_{0.5}FePO_4$, showing domains of $LiFePO_4$ and $FePO_4$ aligned along the *c*-axis. *Right*: High-resolution TEM image with Fourier transforms of the boxed areas, identifying the two phases (Used with permission from Ref. [189])

triphylite are approximated in the figure, because of the uncertainties outlined above. Additionally, due to slow kinetics, the exact temperature boundaries are not known, explaining the differences observed by various researchers. Depending upon the initial concentration, and details of the crystal sizes and morphologies, metastable lithium-deficient phases can persist for remarkably long times after cooling [187].

The mechanism of the $LiFePO_4/FePO_4$ electrochemical reaction has been described using a shrinking core model [188], as depicted in Fig. 2.9. During discharge, lithium initially inserts into $FePO_4$ to form the solid-solution $Li_{\alpha}FePO_4$ phase, where α is close to 0. Upon further passage of current, a shell of a lithium-rich material ($Li_{1-\beta}FePO_4$) is produced on the surface, over a core of $Li_{\alpha}FePO_4$. As the reaction continues to progress, the shell grows at the expense of the core, and the interface between the two phases shrinks, until complete conversion to $Li_{1-\beta}FePO_4$ occurs. Further lithiation produces $LiFePO_4$ at the end-of-discharge. The entire process is reversed upon charge. The anisotropy of lithium diffusion in $LiFePO_4$ [172–174], however, complicates the interpretation of the shrinking core model. A transmission electron microscopy (TEM) study of partially delithiated large plate-like particles [189] show that ordered domains of $FePO_4$ and $LiFePO_4$ alternate in the *ac* plane, separated by narrow disordered (but not amorphous) regions, where lithium mobility is enhanced. The phase transformation proceeds in the direction of the *a*-axis at dislocation lines that run parallel to the *c*-axis, consistent with one-dimensional Li^+ diffusion in the *b*-direction (Fig. 2.11). This somewhat resembles an early "mosaic" model proposed by Andersson et al. as an alternative to the shrinking core model [190]. These observations also suggest that the best rate performance can be achieved with particles that are thin in the direction of Li diffusion (*b*-axis), but that nanostructuring in other directions may not be required.

In another recent study [191] using high-resolution electron energy loss spectroscopy (EELS) on a chemically prepared sample, a different distribution of the two phases in a partially delithiated particle was observed. In this case, $LiFePO_4$ was present only at the edges with $FePO_4$ located in the interior (but not on surfaces of the *ac* planes) of plate-like particles significantly smaller than those studied in Ref. [189]. This is consistent with a progressive emptying or filling of Li channels oriented along the *b*-axis, with the front between the two phases moving perpendicular to the *ac* plane. No disordered regions at the phase boundaries were detected, however. This lack of evidence for solid-solution behavior argues against a shrinking core mechanism, which requires that at least a small degree of non-stoichiometry exist in the system.

Variations in particle sizes and morphologies, as well as in the concentration of defects, may well influence the progression of the delithiation reaction during chemical oxidation and explain these differing results. In electrochemical cells with composite electrodes, the reaction may nucleate preferentially at sites where contact with conductive carbon additives or coatings and the electrolyte solution is the closest, leading to a different pattern of phase distributions than is seen in the chemically delithiated samples, where nucleation can occur at numerous sites simultaneously. In partially delithiated Li_xFePO_4 samples recovered from electrochemical cells, no mixed-phase nanoparticles were observed, leading the researchers to surmise that the reaction front propagates much more rapidly than nucleation [192]. A recent kinetic study also indicates that the $LiFePO_4/FePO_4$ transformation is controlled by a phase-boundary reaction [193]. However, newly discovered evidence of intercrystallite ionic transport, leading to a redox reaction between delithiated and lithiated particles and subsequent equilibration [194] complicates the interpretation of these results. Moreover, areas of composite electrodes with poor electronic connectivity may be electrochemically inactive, leading to islands of unreacted $LiFePO_4$. In that case, all of the lithium will be extracted from $LiFePO_4$ in better connected areas, and mixtures of $FePO_4$ and $LiFePO_4$ will be observed, as in Ref. [192].

While the actual mechanism of the $LiFePO_4/FePO_4$ transformation remains a subject of debate, it seems clear that the shrinking core model does not apply to the primary particles themselves. The model may, however, still be applicable on a larger scale, for example, to the secondary particles comprised of agglomerates.

Over the past decade, better control of synthesis parameters, the use of conductive coatings, and nanostructuring have transformed $LiFePO_4$ from a poorly performing material to one of the most attractive cathodes for Li-ion batteries. $LiFePO_4$ appears to be particularly well suited to high-power applications including power tools and vehicle propulsion. A recent study shows that extraordinarily high charge and discharge currents can be sustained in cells designed so that a modified $LiFePO_4$ limits rate [195]. (While these devices are not practical for real-world use, they serve to demonstrate the intrinsic rate capability of $LiFePO_4$

without interference from mass transfer limitations in other cell components). There have been reports [196, 197] of iron dissolution in $LiPF_6$-containing electrolytes leading to capacity fading at elevated temperatures (analogous to the problems observed with manganese oxide spinels), although this may be due to the presence of iron-containing surface impurities such as Fe_2P rather than to the $LiFePO_4$ itself. The thermal properties of the $LiFePO_4$/$FePO_4$ system are a particularly attractive feature, leading to enhanced safety (LFP, Table 2.2). Upon heating, $FePO_4$ produced by charging $LiFePO_4$ transforms to the thermodynamically favored trigonal form (α-quartz structure). While this reaction is irreversible and leads to loss of capacity, it progresses without evolution of oxygen [198]. This is in contrast to transition metal oxides, all of which lose oxygen to some degree at high states-of-charge. This makes this cathode especially appealing for traction applications, where safety is paramount.

Because $LiFePO_4$ is less dense than the layered oxides or spinels (the crystallographic density is 3.6 g/cm^3 compared to about 5 g/cm^2 for the oxides), and the potential versus lithium is lower, the energy density is less than that of the oxides (Table 2.2). The specific energy, in contrast, is competitive with LMO (Table 2.1), but for many applications, the energy per unit volume matters more than per weight. The discharge potential of the isostructural $LiMnPO_4$ is about 0.5 V versus Li/Li$^+$ higher than that of $LiFePO_4$ [199], which increases the specific energy by about 15%. Unfortunately, this material is even less dense than $LiFePO_4$ (3.4 g/cm^3), and the conductivity appears to be several orders of magnitude lower [200, 201]. Synthetic procedures used to produce nanoparticulate $LiMnPO_4$ and variants include sol-gel, precipitation, combustion techniques, spray pyrolysis, and hydrothermal or solvothermal (polyol process) methods [176, 202–208]. For samples calcined in air for the sake of convenience, a fair amount of carbon is generally added after synthesis to offset the low conductivity. Coating can also be achieved via incorporation of carbonaceous precursors or elemental carbon during heat treatment under inert atmosphere, as with $LiFePO_4$. Electrochemical performance improves as the average primary particle size decreases [209]. Partial Mg substitution on the Mn site is also beneficial [208, 210–212]. This effect has been attributed to stabilization against strain associated with the Jahn–Teller distortion of Mn^{3+} ions in the delithiated phase, as well as decreased volume changes upon cycling. The best results reported so far have been for solvothermally prepared powders (polyol process) embedded in a carbon matrix [213]. Still, the rate capability of $LiMnPO_4$ is not as impressive as that of $LiFePO_4$, and many of the strategies employed to improve the electrochemistry (Mg substitution, addition of large amounts of carbon, nanostructuring) reduce the already fairly small energy density advantage. The disappointing performance has been variously attributed to poor transport properties in either the bulk $LiMnPO_4$ or $MnPO_4$ phases, the instability of the $MnPO_4$ phase itself, or surface effects [201, 214, 215]. While the voltage profile of $LiMnPO_4$ is flat during charge and discharge, indicating a two-phase process, evidence of solid-solution behavior near the $MnPO_4$ limit has been observed [216]. As with the $LiFePO_4$/$FePO_4$ system, the non stoichiometry may enable the electrochemical activity. However, no solid-solution behavior near the $LiMnPO_4$ end of the phase diagram has yet been detected.

Although the performance characteristics of the $LiMnPO_4/MnPO_4$ system may improve with further work, one troubling aspect of this electrode is its thermal instability in the charged state. Unlike $LiFePO_4$, $MnPO_4$ evolves oxygen gas upon heating to 200°C and decomposes to form $Mn_2P_2O_7$ [217, 218]. The instability of $MnPO_4$ is probably related to the strong Jahn–Teller distortion of the Mn^{3+} ion. $LiMnPO_4$ is therefore less attractive than $LiFePO_4$ in terms of safety, and does not have better performance characteristics than the metal oxides. Charging is also somewhat problematic, because high over-potentials are required due to the kinetic limitations. Thus, it seems unlikely that this cathode material will prove useful for traction batteries in the near term, although other applications may be feasible.

Phospho-olivine compounds containing Co or Ni also exist. $LiCoPO_4$ exhibits electrochemical activity at about 4.8 V versus Li/Li^+ [219, 220]. $LiNiPO_4$ is predicted to discharge at about 5.1 V in a lithium cell, but appears to be nearly completely inactive [221]. Neither of these is likely to be used as cathodes for lithium-ion batteries in the near term in part because of the very high voltages needed to charge the materials, which present a number of practical problems.

Solid solutions containing a mixture of transition metals can be prepared over a wide composition range [176]. $Li[Mn_yFe_{1-y}]PO_4$ compounds exhibit two plateaus in the discharge profile at about 4.1 and 3.45 V versus Li/Li^+ with their relative magnitudes proportional to the amounts of Mn and Fe, respectively [148]. In general, for $y < 0.8$, the mixed metal phospho-olivines appear to undergo more facile electrochemical reactions than the pure end-member phase, $LiMnPO_4$ [215, 222]. A study of the delithiation reactions of these phases [223] suggested that the system is single phase when $x < 1-y$, but biphasic over the 4.1 V plateau (corresponding to the Mn^{2+}/Mn^{3+} redox couple). A later synchrotron diffraction study [224] showed two two-phase regions roughly coinciding with the two plateaus and a narrow solid-solution region between $x = 0.55$ and 0.67 for $Li_xMn_{0.6}Fe_{0.4}PO_4$, corresponding to the steeply sloping portion of the discharge profile between the plateaus.

Other mixed transition metal phospho-olivines have been prepared containing Ni and Co [220] and Fe, Mn, and Co [225–227]. In the case of the $Li[Ni_yCo_{1-y}]PO_4$, only one plateau was observed at 4.8 V, corresponding to the Co^{2+}/Co^{3+} redox couple. The only effect of the Ni substitution is to reduce the overall capacity, demonstrating the poor electro-activity of Ni in the phospho-olivine structure. In lithium cells containing $LiMn_{1/3}Fe_{1/3}Co_{1/3}PO_4$, on the other hand, three distinct electrochemical features are observed, corresponding to redox processes of the three types of transition metals (Fig. 2.12). Interestingly, the reaction appears to be single phase over the entire composition range, $0 \leq x \leq 1$ in $LiMn_{1/3}Fe_{1/3}Co_{1/3}PO_4$, and the redox potentials of the Fe^{2+}/Fe^{3+} and Co^{2+}/Co^{3+} couples are slightly shifted compared to the corresponding $LiMPO_4$ electrodes containing only one metal. The manganese redox processes appear to be more sluggish than those of iron and cobalt, and at higher discharge rates, the electrochemical feature at 4.1 V disappears. Tailoring of the voltage profile by incorporating multiple metals in the

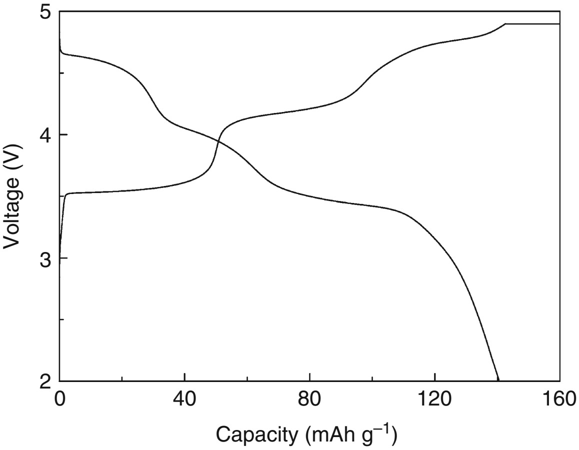

Fig. 2.12 Charge and discharge of a Li/$LiMn_{1/3}Fe_{1/3}Co_{1/3}PO_4$ cell, showing three distinct plateaus corresponding to the redox of Co (4.8 V), Mn (4.1 V), and Fe (3.45 V) (Used with permission from Refs. [225–227])

olivine structure may have practical use as a state-of-charge indicator for vehicular batteries (acting much like the gas gauge in conventional combustion engine automobiles).

Other Phosphates and Poly-anionic Compounds

There are many other transition metal-containing poly-anionic compounds with structures amenable to lithium insertion processes. Among these are numerous materials with the Nasicon structure (Nasicon stands for sodium superionic conductor and originally referred to $Na_{1+x}Zr_2P_{3-y}Si_yO_{12}$ compounds [228]). These have the general formula $A_xM_2(XO_4)_3$, where A is an alkali metal or alkaline earth, M is a transition metal or combination of transition metals, and X is P, As, Si, or S or a combination of these. M is octahedrally coordinated by oxygen, and X is tetrahedrally coordinated. All corners of the XO_4 tetrahedra are shared with MO_6 octahedra and vice versa; these link to form open channels in which the alkali or alkaline earth ions are located. There are also closely related three-dimensional framework structures with differing arrangements of corner-sharing polyhedra and distributions of alkali metal cations, such as the monoclinic $Li_3Fe_2(PO_4)_3$ shown in Fig. 2.13.

Transport of alkali metal ions through the tunnels in Nasicons can be extremely rapid, particularly at elevated temperatures, although the electronic conductivities are low. For these reasons, these materials were originally proposed for use as solid ionic conductors (e.g., to replace β'' alumina in high temperature Na/S batteries). In spite of their low electronic conductivities, researchers recognized that Nasicon structures with redox-active transition metals and related three-dimensional framework compounds could function as electrode materials as early as the late 1980s [229–231] and numerous materials were investigated [232, 233]. In many cases, the electrochemical

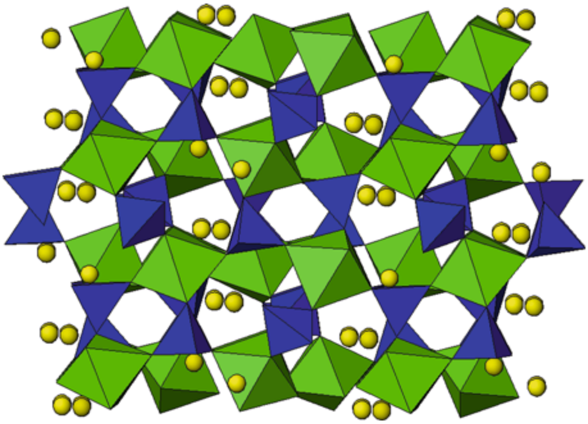

Fig. 2.13 The structure of monoclinic $Li_3Fe_2(PO_4)_3$ looking down the unique axis. P is located in the blue tetrahedra, and Fe in the *green* octahedra. Li ions are represented as spheres

properties are unsuitable for Li-ion batteries. For example, Li cannot be extracted from monoclinic $Li_3Fe_2(PO_4)_3$, only inserted, and the discharge occurs at a rather low voltage (2.8 V versus Li/Li^+). In contrast, up to two lithiums per formula unit can be extracted reversibly from monoclinic $Li_3V_2(PO_4)_3$, corresponding to a capacity of about 130 mAh/g at an average potential of 3.8 V [234–236]. Complex multiphasic behavior is exhibited upon redox, resulting in multiple plateaus in the discharge profile. In spite of significant volume changes upon lithium insertion and extraction, the material shows very good cycling behavior.

Fluorophosphates are relatively rare, but have recently been studied for Li-ion applications. The lithium in $LiVPO_4F$ [237–239] can be extracted reversibly at a potential of about 4.2 V versus Li/Li^+. Interestingly, lithium can also be inserted at about 1.8 V. Thus, a graphite-free lithium-ion battery can be built, using $LiVPO_4F$ as both the anode and the cathode! $Na_3V_2(PO_4)_2F_3$ [240], Na_2FePO_4F [241], and $LiFePO_4F$ [242, 243] have also been investigated. The first two compounds were used as-is in electrochemical cells, and underwent ion exchange in situ. Although these cathodes eventually stabilize when used in lithium metal cell configurations and the cycling behavior is good, the presence of sodium in full cells with graphite anodes may disrupt the SEI layer and is therefore undesirable. Thus, these compounds will have to be ion-exchanged prior to use. In the case of $LiFePO_4F$, the investigators saw some evidence that a small amount of lithium could be extracted (with concomitant oxidation of Fe^{3+} to Fe^{4+}), but the main electrochemical reaction was insertion of lithium and reduction of Fe^{3+} to Fe^{2+}.

Other electroactive phosphorus-containing compounds include iron(III) hydroxyl phosphates with lipscombite or tavorite structures [244, 245], β- and ε-$VOPO_4$ [246–248], and $LiVP_2O_7$ [249]. Although the Nasicons, three-dimensional framework structures, and the aforementioned phosphates and diphosphates all have interesting electrochemical properties, most are not competitive with $LiFePO_4$ or the commercialized metal oxides for a variety of reasons. The iron-containing materials generally discharge at too low a voltage for use in Li-ion battery

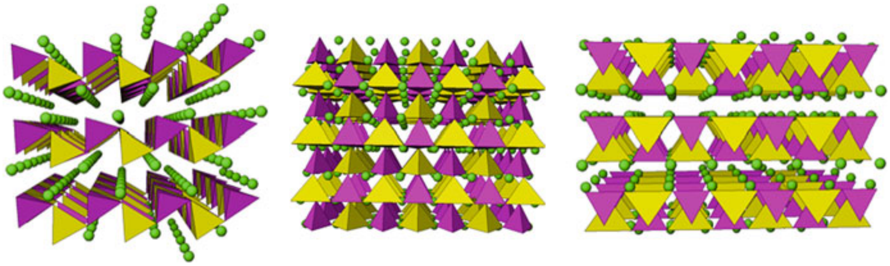

Fig. 2.14 Views of a β-polymorph of Li_2MSiO_4 looking down the *a*-axis (*left*), the *b*-axis (*middle*), and the *c*-axis (*right*). MO_4 (*yellow*) and SiO_4 (*pink*) tetrahedra alternate and connect to form layers through which lithium ions (*green spheres*) can diffuse

configurations and many have fairly low capacities. Some would need to be lithiated prior to use. The vanadium-containing materials cycle well, and have sufficiently high voltages and capacities to ensure high energy density, but raise concerns about toxicity and environmental impact.

Interest has also recently been directed toward a family of silicates with the general composition Li_2MSiO_4, where M is a divalent cation such as Fe^{2+}, Mn^{2+}, and Co^{2+} or a combination of these [250–257]. The chemical formula implies that it may be possible to extract two Li ions per transition metal unit, giving a very high theoretical specific capacity of about 330 mAh/g. These materials adopt structures in which Li, Si, and the transition metal ions all occupy tetrahedral sites in a distorted close-packed oxygen array. The particular polymorph obtained depends upon the nature of the transition metal as well as the temperature and method of preparation. In the β-polymorphs (low-temperature forms), the tetrahedra share only corners, and all point in the same direction. In γ-polymorphs (high temperature forms), triads of tetrahedra are arranged so that the central one points in the opposite direction and shares edges with the two outer tetrahedra. Numerous tetrahedral structures exist, with different ordering of the ions and varying degrees of distortion. Several different views of an electroactive β-polymorph (space group $Pmn2_1$) are shown in Fig. 2.14, which illustrates its quasi-layered nature. Accurate structure determination of these phases is complicated by the presence of impurities in many preparations and variations in synthetic procedures, which may lead to subtle structural differences [256, 258].

About one Li^+ per formula unit can be extracted from Li_2FeSiO_4 in electrochemical cells at low current densities and at 60°C [250, 251]. The initial extraction takes place at about 3.1 V versus Li/Li^+, but subsequent discharges and charges occur at 2.8 V. This indicates that a structural change takes place, the exact nature of which is not entirely clear. After this initial change, however, relatively good cycling is observed, with an overall capacity of about 130 mAh/g (corresponding to somewhat less than 1 Li^+ per Li_2FeSiO_4). There is no experimental evidence that more than one Li^+ can be extracted, and first principle calculations indicate that it is not possible to do so at potentials compatible with conventional organic liquid electrolytes [259].

The differences between the potentials at which the first and second lithium ions can be extracted are much smaller when M=Mn, Co, or Ni in Li_2MSiO_4 than when it is Fe, however. As with the olivine system, the redox potentials for Li_2MnSiO_4 electrochemical processes (at least for extraction of the first lithium) are expected to be within the oxidative stability limits of organic electrolytes, while those of Li_2CoSiO_4 and Li_2NiSiO_4 are probably not. However the electrochemical behavior of Li_2MnSiO_4 appears to be much worse than that of Li_2FeSiO_4 [251, 254]. Belharaouk et al. [253] were able to achieve initial discharge capacities of about 135 mAh/g at room temperature, over a wide voltage range, by using carbon-coated submicron-sized particles, but this is still far less than predicted for complete extraction of all the lithium. Discharge capacities as high as about 250 mAh/g, however, can be obtained when mixed metal compounds $Li_2Mn_xFe_{1-x}SiO_4$ [252, 256] are used as cathodes in lithium cells. Unfortunately, the quality of the energy obtained is poor because the voltage profiles are steeply sloping over a range of about 4.5–1.0 V versus Li/Li^+. At such low potentials, relatively little power can be obtained from the electrode. The extreme slope may be partly due to the severe kinetic and electronic limitations of the materials, leading to large over-potentials in lithium cells. If so, a combination of the carbon-coating and nanostructuring strategies used to improve the olivines may ameliorate the poor voltage characteristics and lead to new cathodes with nearly double the energy currently available.

Conversion Electrodes

A different class of electrode materials is based not upon insertion processes but on the displacement reactions of binary metal compounds [260, 261] (Eq. 2.4):

$$\mathrm{nLi^+ + ne^- + M^{n+}X_m \leftrightarrow M + nLiX_{m/n} (X = O, F, N, S)} \tag{2.4}$$

Conversion electrodes have long been used in primary systems (e.g., Li/CF_x batteries), but have only been proposed for use in rechargeable devices recently, when it was recognized that the reactions could be made reversible for nanoparticulate materials. While the specific capacities can be enormous, the voltage characteristics make most of these electrodes more suitable for use as anodes rather than as cathodes. A notable exception seems to be that of metal fluorides, which are electroactive anywhere from 2 to 4 V versus Li/Li^+, depending on the identity of the metal, with specific capacities as high as 600 mAh/g. It is typical of conversion electrodes to exhibit significant hysteresis upon recharge, which may be intrinsic to the materials and processes. The mechanisms of conversion reactions are complex and involve bond breaking and considerable rearrangement, unlike that of insertion electrodes. The reassembly of the original phase upon recharge does not necessarily involve the same kinetic pathways and intermediates as the production of the elemental metal and LiF during discharge. Thus, it may not be possible to remove the hysteresis entirely either by engineering of devices or by improving the material properties to ensure faster rate capability. This property has an adverse effect on the round-trip efficiencies, and may make conversion electrodes unsuitable for Li-ion batteries unless a solution can be found to this problem.

Future Directions

Because none of the cathode materials discussed above are ideal for every application, the search for new insertion electrodes continues. Batteries are relatively simple devices, but the simultaneous requirements for high energy density, long cycle life, safety, and low cost impose stringent restrictions upon the choices available for cathode materials. The highly successful example of $LiFePO_4$ has directed researchers toward the exploration of other poly-anionic compounds that may share its excellent thermal stability at high states of charge. It is now evident that nanostructuring and/or conductive coatings can overcome kinetic and electronic limitations, allowing materials that would once have been thought of as unsuitable for electrodes to be considered. Changes in the phase behavior of nanoparticulate materials (in comparison to the conventionally sized powders) can render compounds electroactive that, in bulk form, appear to be unpromising due to their insulating nature. The shortened diffusion distances for lithium in nanoparticles may enable high rate capability in powders that appear to have severe rate limitations when micron-sized or larger. While this allows the menu of potential cathodes to be greatly expanded, the concept of “going nano” should be approached with caution. It is most successful when it is applied to materials that undergo redox well within the electrolyte stability range, such as with $LiFePO_4$. The increased surface area of nanoparticulate powders compared to conventionally sized materials exacerbates any tendency toward irreversible reaction with electrolytes. In addition to the very serious safety concerns this raises, the paradoxical result may be to lower rate capability due to the increased presence of resistive reaction layers on cathode particle surfaces [262]! Nano-sizing may also adversely impact practical specific energies because processing into electrodes becomes more difficult. It is often necessary, for example, to add more carbon to the composite cathode to ensure good electrical connectivity, but this contributes dead weight. High surface area particles also do not pack well, leading to decreases in the tap densities and lower energy densities. Ensuring that nanoparticles are regularly shaped rather than irregularly can ameliorate these tendencies, however [263]. Another potentially useful approach is to synthesize mesoporous materials [264] in which the particles are micron-sized but contain pores of controlled sizes and distributions so as to maximize contact between the electrolyte and active material. This effectively shortens diffusion distances, while minimizing the tap density effects and maintaining the ease of electrode processing.

The use of nano metric or very thin coatings on cathode particle surfaces to improve the electronic conductivity of a material, to decrease dissolution, suppress oxygen loss, or to extend the operating voltage range is somewhat less problematic than simply nano-sizing cathode powders. In principle, this may allow using a wider variety of materials, including high-voltage/high-energy electrodes safely, without compromising cycle life or requiring the use of exotic electrolytes. Here the challenge is to identify and prepare coatings that prevent contact with electrolyte, yet allow the transport of lithium ions. They must also remain essentially defect-free over many cycles in which the cathode particles may undergo significant volume changes. A related concept is the preparation of "core-shell" or compositionally graded materials in which two or more compounds are combined in the same particle [265]. The core of the material can be a high-capacity material and the outer shell one that has lower energy but better thermal stability, for example. A difficulty is the tendency for the shell to become detached from the core if the volume changes upon cycling are not carefully matched. A compositionally graded material is less subject to these stresses, but more complex to prepare.

Researchers continue to look for materials that can deliver higher capacities and energies than those currently available. The layered-layered composite materials (i.e., the solid solutions between Li_2MnO_3 and $LiNi_{0.5}Mn_{0.5}O_2$ or $LiNi_xCo_{1-2x}Mn_xO_2$), which are very high capacity once they are activated in electrochemical cells, are a recent promising development. Cathodes that can undergo more than one oxidation state change per metal center reversibly could substantially increase the capacity of lithium-ion batteries. These include the Li_2MSiO_4 compounds and conversion electrodes discussed above, but these require much more work before they can be envisioned for use in lithium-ion batteries.

The challenges presented by these new materials illustrate the delicate balance of performance characteristics, cost, and safety that the battery electrode designer must be able to meet. There is now renewed interest among researchers in lithium metal batteries, because of the very high energy densities that might be achieved. However, now instead of intercalation electrodes, developers are reconsidering the use of sulfur and air (oxygen) cathodes for lithium metal batteries intended for vehicles. The extremely high theoretical capacities of these materials (e.g., over 1,600 mAh/g for sulfur) in lithium batteries are certainly tantalizing, but the difficulties associated with their use have proven daunting. In the case of sulfur, LiS_x intermediates dissolve in the electrolyte solutions, eventually migrating to the lithium anode and precipitating as Li_2S. The development of the protected lithium electrode (PLE) by PolyPlus Battery Company (Berkeley, CA) has extended the cycle life significantly, and Li/S batteries are now used for some military applications. In PLEs, the lithium anode is covered by a thin dense protective film (e.g., a lithium-ion conducting ceramic such as Lisicon, a ceramic with the Nasicon structure), which not only prevents contact with soluble intermediates but also with the electrolyte. An interlayer between the lithium and the protective layer is also needed to prevent reduction of the latter. Thus, in principle, it is possible to operate lithium cells with a wide variety of electrolytes, including aqueous ones. A lithium/water battery has even been developed for niche applications, although it is intended for use only as a primary, at present.

While in principle it should be possible to operate a lithium/air battery using a PLE to prevent contact of lithium with adventitious water and CO_2 in the atmosphere, rechargeable systems have so far eluded success. The reduction of oxygen itself is somewhat sluggish, necessitating the use of a catalyst. The Li_2O_2, which is the reaction product when nonaqueous electrolytes are used, precipitates out during discharge and eventually clogs the pores of the air electrode structure. While some researchers have claimed to have successfully recharged a lithium/air battery, the large hysteresis observed suggests that a side-reaction involving the electrolyte is responsible for the charging behavior instead of reoxidation of Li_2O_2 to oxygen.

Ultimately, the success or failure of lithium/sulfur or air systems, however, hinges upon convincing demonstration of safe and reliable operation of the lithium anode over the many cycles required for applications requiring rechargeable devices.

Acknowledgments This work was supported by the Assistant Secretary for Energy Efficiency and Renewable Energy, Office of Vehicle Technologies of the US Department of Energy under Contract No. DE-AC02-05CH11231. The author would like to thank Dr. Kinson Kam, Dr. Jordi Cabana, and Mr. Thomas Conry for helpful discussion.

Bibliography

Primary Literature

1. Whittingham MS, Gamble FR (1975) The lithium intercalates of the transition metal dichalcogenides. Mat Res Bull 10:363–372
2. Whittingham MS (1976) The role of ternary phases in cathode reactions. J Electrochem Soc 123:315–320
3. Whittingham MS (1978) Chemistry of intercalation compounds: metal guests in chalcogenide hosts. Prog Solid Stat Chem 12:41–99
4. Mizushima K, Jones PC, Wiseman PJ, Goodenough JB (1980) Li_xCoO_2 ($0 \leq x \leq 1$): a new cathode material for batteries of high energy density. Mat Res Bull 15:783–799
5. Goodenough JB (2007) Cathode materials: a personal perspective. J Power Sources 174:996–1000
6. Dresselhaus MS, Dresselhaus G (1981) Intercalation compounds of graphite. Adv Phys 30:139–326
7. Fong R, von Sacken U, Dahn JR (1990) Studies of lithium intercalation into carbons using nonaqueous electrochemical cells. J Electrochem Soc 137:2009–2013
8. Nagaura T, Tozawa K (1990) Lithium ion rechargeable battery. Prog Batteries Sol Cells 9:209–219
9. Akridge J, Brodd R (2010) Li-ion markets. In: Pacific power symposium, Waikoloa, HI
10. Srinivasan V (2008) Batteries for vehicular applications. In: AIP conference proceedings physics of sustainable energy, Berkeley, CA, vol 1044, pp 283–296
11. Karden E, Ploumen S, Fricke B, Miller T, Snyder K (2007) Energy storage devices for future hybrid electric vehicles. J Power Sources 168:2–11
12. Chalk SG, Miller JF (2006) Key challenges and recent progress in batteries, fuel cells, and hydrogen storage for clean energy systems. J Power Sources 159:73–80
13. Gaines L, Cuenca R (2000) Costs of lithium-ion batteries for vehicles. Report, Center for Transportation Research, Argonne National Laboratory, Argonne

14. Murphy DW, Christian PA (1979) Solid state electrodes for high energy batteries. Science 205:651–656
15. Ohzuku T, Ueda A (1994) Solid-state redox reactions of $LiCoO_2$ (R-3m) for 4 volt secondary lithium cells. J Electrochem Soc 141:2972–2977
16. Reimers JN, Dahn JR (1992) Electrochemical and in situ diffraction studies of lithium intercalation in Li_xCoO_2. J Electrochem Soc 139:2091–2097
17. Chen Z, Lu Z, Dahn JR (2002) Staging phase transitions in Li_xCoO_2. J Electrochem Soc 149: A1604–A1609
18. Aurbach D, Markovsky B, Rodkin A, Levi E, Cohen YS, Kim H-J, Schmidt M (2002) On the capacity fading of $LiCoO_2$ intercalation electrodes: the effect of cycling, storage, temperature, and surface film forming additives. Electrochim Acta 47:4291–4306
19. Amatucci GG, Tarascon JM, Klein LC (1996) CoO_2, The end member of the Li_xCoO_2 solid solution. J Electrochem Soc 143:1114–1123
20. Van der Ven A, Aydinol MK, Ceder G (1998) First-principles evidence for stage ordering in Li_xCoO_2. J Electrochem Soc 145:2149–2155
21. Xia H, Lu L, Meng YS, Ceder G (2007) Phase transitions and high voltage electrochemical behavior of $LiCoO_2$ thin films grown by pulsed laser deposition. J Electrochem Soc 154: A337–A342
22. Cho J, Kim G (1999) Enhancement of thermal stability of $LiCoO_2$ by $LiMn_2O_4$ coating. Electrochem Solid-State Lett 2:253–255
23. Kim B, Kim C, Kim T-G, Ahn D, Park B (2006) The effect of $AlPO_4$-coating layer on the electrochemical properties in $LiCoO_2$ thin films. J Electrochem Soc 153:A1773–A1777
24. Chen Z, Dahn JR (2004) Methods to obtain excellent capacity retention in $LiCoO_2$ cycled to 4.5V. Electrochim Acta 49:1079–1090
25. Thomas MGSR, David WIF, Goodenough JB (1985) Synthesis and structural characterization of the normal spinel $Li[Ni_2O_4]$. Mat Res Bull 20:1137–1146
26. Dahn JR, von Sacken U, Michal CA (1990) Structure and electrochemistry of $Li_{1\pm y}NiO_2$ and a new Li_2NiO_2 phase with the $Ni(OH)_2$ structure. Sol State Ionics 44:87–97
27. Broussely M, Perton F, Biensan P, Bodet JM, Labat J, Lecerf A, Delmas C, Rougier A, Pérès JP (1995) Li_xNiO_2, a promising cathode for rechargeable lithium batteries. J Power Sources 54:109–114
28. Dahn JR, von Sacken U, Juzkow MW, Al-Janaby H (1991) Rechargeable $LiNiO_2$/carbon cells. J Electrochem Soc 138:2207–2211
29. Rougier A, Gravereau P, Delmas C (1996) Optimization of the composition of the $Li_{1-z}Ni_{1+z}O_2$ electrode materials: structural, magnetic, and electrochemical studies. J Electrochem Soc 143:1168–1175
30. Pérès JP, Delmas C, Rougier A, Broussely M, Perton F, Biensan P, Willman P (1996) The relationship between the composition of lithium nickel oxide and the loss of reversibility during the first cycle. J Phys Chem Solids 57:1057–1060
31. Delmas C, Pérès JP, Rougier A, Demourgues A, Weill F, Chadwick A, Broussely M, Perton F, Biensan P, Willman P (1997) On the behavior of the Li_xNiO_2 system: an electrochemical and structural overview. J Power Sources 68:120–125
32. Ohzuku T, Ueda A, Nagayama M, Iwakoshi Y, Komori H (1993) Comparative study of $LiCoO_2$, $LiNi_{1/2}Co_{1/2}O_2$ and $LiNiO_2$ for 4 volt secondary lithium cells. Electrochim Acta 38:1159–1167
33. Dahn JR, Fuller EW, Obrovac M, von Sacken U (1994) Thermal stability of Li_xCoO_2, Li_xNiO_2 and λ-MnO_2 and consequences for the safety of Li-ion cells. Sol State Ionics 69:265–270
34. Ohzuku T, Ueda A, Kouguchi M (1995) Synthesis and characterization of $LiAl_{1/4}Ni_{3/4}O_2$ (R-3m) for lithium-ion (Shuttlecock) batteries. J Electrochem Soc 142:4033–4439
35. Arai H, Sakurai Y (1999) Characteristics of Li_xNiO_2 obtained by chemical delithiation. J Power Sources 81–82:401–405

36. Albrecht S, Kümpers J, Kruft M, Malcus S, Vogler C, Wahl M, Wohlfahrt-Mehrens M (2003) Electrochemical and thermal behavior of aluminum- and magnesium-doped spherical lithium nickel cobalt mixed oxides $Li_{1-x}(Ni_{1-y-z}Co_yM_z)O_2$ (M=Al, Mg). J Power Sources 119–121:178–183
37. Onnerud PT, Shi JJ, Dalton SL, Lampe-Onnerud C (2008) Lithium metal oxide materials and methods of synthesis and use. US Patent 2008/0286460 A1
38. Chen CH, Liu J, Stoll ME, Henriksen G, Vissers DR, Amine K (2004) Aluminum-doped lithium nickel cobalt oxide electrodes for high-power lithium-ion batteries. J Power Sources 128:278–285
39. Kostecki R, Lei J, McLarnon F, Shim J, Striebel K (2006) Diagnostic evaluation of detrimental phenomena in high-power lithium-ion batteries. J Electrochem Soc 153:A669–A672
40. Tabuchi M, Tsutsui S, Masquelier C, Kanno R, Ado K, Matsubara I, Nasu S, Kageyama H (1998) Effect of cation arrangement on the magnetic properties of lithium ferrites ($LiFeO_2$ prepared by hydrothermal reaction and post-annealing method). J Solid State Chem 140:159–167
41. Ado K, Tabuchi M, Kobayashi H, Kageyama H, Nakamura O, Inaba Y, Kanno R (1997) Preparation of $LiFeO_2$ with alpha-$NaFeO_2$-type structure using a mixed-alkaline hydrothermal method. J Electrochem Soc 144:L177–L180
42. Kanno R, Shirane T, Kawamoto Y, Takeda Y, Takano M, Ohashi M, Yamaguchi Y (1996) Synthesis, structure, and electrochemical properties of a new lithium iron oxide, $LiFeO_2$, with a corrugated layer structure. J Electrochem Soc 143:2435–2442
43. Morales J, Santos-Peña J (2007) Highly electroactive nanosized α-$LiFeO_2$. Electrochem Commun 9:2116–2120
44. Johnson CS, Kang S-H, Vaughey JT, Pol SV, Balasubramanian M, Thackeray MM (2010) Li_2O Removal from Li_5FeO_4: a cathode precursor for lithium-ion batteries. Chem Mater 22:1263–1270
45. Armstrong AR, Bruce PG (1996) Synthesis of layered $LiMnO_2$ as an electrode for rechargeable lithium batteries. Nature 381:499–500
46. Thackeray MM (1997) Manganese oxides for lithium batteries. Prog Solid State Chem 25:1–71
47. Reed J, Ceder G (2004) Role of electronic structure in the susceptibility of metastable transition-metal oxide structures to transformation. Chem Rev 104:4513–4534
48. Paulsen JM, Thomas CL, Dahn JR (1999) Layered Li-Mn-oxide with the O2 structure: a cathode material for Li-Ion cells which does not convert to spinel. J Electrochem Soc 146:3560–3565
49. Eriksson TA, Lee YJ, Hollingsworth J, Reimer JA, Cairns EJ, Zhang X-F, Doeff MM (2003) Influence of substitution on the structure and electrochemistry of layered manganese oxides. Chem Mater 15:4456–4463
50. Dollé M, Patoux S, Doeff MM (2005) Layered manganese oxide intergrowth electrodes for rechargeable lithium batteries. 1. substitution with Co or Ni. Chem Mater 17:1036–1043
51. Patoux S, Dollé M, Doeff MM (2005) Layered manganese oxide intergrowth electrodes for rechargeable lithium batteries. 2. substitution with Al. Chem Mater 17:1044–1054
52. Robertson AD, Armstrong AR, Bruce PG (2000) Influence of ion exchange conditions on the defect chemistry and performance of cobalt doped layered lithium manganese oxide based intercalation compounds. Chem Commun 20:1997–1998
53. Doeff MM, Peng MY, Ma Y, De Jonghe LC (1994) Orthorhombic Na_xMnO_2 as a cathode material for secondary sodium and lithium polymer batteries. J Electrochem Soc 141:L145–L147
54. Doeff MM, Richardson TJ, Kepley L (1996) Lithium insertion processes of orthorhombic Na_xMnO_2-base electrode materials. J Electrochem Soc 143:2507–2516
55. Hu F, Doeff MM (2004) Electrochemical characterization of manganese oxide cathode materials based on $Na_{0.4}MnO_2$. J Power Sources 129:296–302
56. Armstrong AR, Huang H, Jennings RA, Bruce PG (1998) $Li_{0.44}MnO_2$: an intercalation electrode with a tunnel structure and excellent cyclability. J Mater Chem 8:255–259

57. Doeff MM, Anapolsky A, Edman L, Richardson TJ, De Jonghe LC (2001) A high-rate manganese oxide for rechargeable lithium battery applications. J Electrochem Soc 148: A230–A236
58. Akimoto J, Awaka J, Takahashi Y, Kijima N, Tabuchi M, Nakashima A, Sakaebe H, Tatsumi K (2005) Synthesis and electrochemical properties of $Li_{0.44}MnO_2$ as a novel 4 V cathode material. Electrochem Solid-State Lett 8:A554–A557
59. Kalyani P, Chitra S, Mohan T, Gopukumar S (1999) Lithium metal rechargeable cells using Li_2MnO_3 as the positive electrode. J Power Sources 80:103–106
60. Yu DYW, Yanagida K, Kato Y, Nakamura H (2009) Electrochemical activities in Li_2MnO_3. J Electrochem Soc 156:A417–A424
61. Rossouw MH, Thackeray MM (1991) Lithium manganese oxides from Li_2MnO_3 for rechargeable lithium battery applications. Mat Res Bull 26:463–473
62. Paik Y, Grey CP, Johnson CS, Kim J-S, Thackeray MM (2002) Lithium and deuterium NMR studies of acid-leached layered lithium manganese oxides. Chem Mater 14:5109–5115
63. Storey C, Kargina I, Grincourt Y, Davidson IJ, Yoo YC, Seung DY (2001) Electrochemical characterization of a new high capacity cathode. J Power Sources 97–98:541–544
64. Ammundsen B, Paulsen J, Davidson I, Liu R-S, Shen C-H, Chen J-M, Jang L-Y, Lee J-F (2002) Local structure and first cycle redox mechanism of layered $Li_{1.2}Cr_{0.4}Mn_{0.4}O_2$ cathode material. J Electrochem Soc 149:A431–A436
65. Ohzuku T, Makimura Y (2001) Layered lithium insertion material of $LiNi_{1/2}Mn_{1/2}O_2$: a possible alternative to $LiCoO_2$ for advanced lithium-ion batteries. Chem Lett 8:744–745
66. Rossen E, Jones CDW, Dahn JR (1992) Structure and electrochemistry of $Li_xMn_yNi_{1-y}O_2$. Solid State Ionics 57:311–318
67. Makimura Y, Ohzuku T (2003) Lithium insertion material of $LiNi_{1/2}Mn_{1/2}O_2$ for advanced lithium-ion batteries. J Power Sources 119–121:156–160
68. Lu Z, MacNeil DD, Dahn JR (2001) Layered cathode materials $Li[Ni_xLi_{(1/3-2x/3)}Mn_{(2/3-x/3)}]O_2$ for lithium-ion batteries. Electrochem Solid State Lett 4:A191–A194
69. Reed J, Ceder G (2002) Charge, potential, and phase stability of layered $Li(Ni_{0.5}Mn_{0.5})O_2$. Electrochem Solid-State Lett 5:A145–A148
70. Yoon W-S, Grey CP, Balasubramanian M, Yang X-Q, McBreen J (2003) In situ x-ray absorption spectroscopic study on $LiNi_{0.5}Mn_{0.5}O_2$ cathode material during electrochemical cycling. Chem Mater 15:3161–3169
71. Van der Ven A, Ceder G (2004) Ordering in $Li_x(Ni_{0.5}Mn_{0.5})O_2$ and its relation to charge capacity and electrochemical behavior in rechargeable lithium batteries. Electrochem Commun 6:1045–1050
72. Yoon W-S, Paik Y, Yang X-Q, Balasubramanian M, McBreen J, Grey CP (2002) Investigation of the local structure of the $LiNi_{0.5}Mn_{0.5}O_2$ cathode material during electrochemical cycling by x-ray absorption and NMR spectroscopy. Electrochem Solid State Lett 5: A263–A266
73. Lu Z, Beaulieu LY, Donaberger RA, Thomas CL, Dahn JR (2002) Synthesis, structure, and electrochemical behavior of $Li[Ni_xLi_{1/3-2x/3}Mn_{2/3-x/3}]O_2$. J Electrochem Soc 149: A778–A791
74. Kang S-H, Park S-H, Johnson CS, Amine K (2007) Effects of Li content on structure and electrochemical properties of $Li_{1+x}(Ni_{0.5}Mn_{0.5})_{1-x}O_2$ $(0 \leq x \leq 0.15)$ electrodes in lithium cells (1.0-4.8 V). J Electrochem Soc 154:A268–A274
75. Kang K, Meng YS, Bréger J, Grey CP, Ceder G (2006) Electrodes with high power and high capacity for rechargeable lithium batteries. Science 311:977–980
76. Yabuuchi N, Ohzuku T (2003) Novel lithium insertion material of $LiCo_{1/3}Ni_{1/3}Mn_{1/3}O_2$ for advanced lithium-ion batteries. J Power Sources 119–121:171–174
77. Koyama Y, Tanaka I, Adachi H, Makimura Y, Ohzuku T (2003) Crystal and electronic structures of superstructural $Li_{1-x}[Co_{1/3}Ni_{1/3}Mn_{1/3}]O_2$ $(0 \leq x \leq 1)$. J Power Sources 119–121:644–648

78. Hwang BJ, Tsai YW, Carlier D, Ceder G (2003) A combined computational/experimental study on $LiNi_{1/3}Co_{1/3}Mn_{1/3}O_2$. Chem Mater 15:3676–3682
79. Kim J-M, Chung H-T (2003) The first cycle characteristics of $Li[Ni_{1/3}Co_{1/3}Mn_{1/3}]O_2$. Electrochim Acta 49:937–944
80. Kobayashi H, Arachi Y, Emura S, Kageyama H, Tatsumi K, Kamiyama T (2005) Investigation on lithium de-intercalation mechanism for $Li_{1-y}Ni_{1/3}Mn_{1/3}Co_{1/3}O_2$. J Power Sources 146:640–644
81. Tsai YW, Hwang BJ, Ceder G, Sheu HS, Liu DG, Lee JF (2005) In-situ x-ray absorption spectroscopic study on variation of electronic transitions and local structure of $LiNi_{1/3}Co_{1/3}Mn_{1/3}O_2$ cathode material during electrochemical cycling. Chem Mater 17:3193–3199
82. Kim MG, Shin HJ, Kim J-H, Park S-H, Sun Y-K (2005) XAS investigation of inhomogeneous metal-oxygen bond covalency in bulk and surface for charge compensation in Li-ion battery cathode $Li[Ni_{1/3}Co_{1/3}Mn_{1/3}]O_2$ material. J Electrochem Soc 152:A1320–A1328
83. Yoon W-S, Balasubramanian M, Chung KY, Yang X-Q, McBreen J, Grey CP, Fischer DA (2005) Electrochemical Li-ion deintercalated $Li_{1-x}Co_{1/3}Ni_{1/3}Mn_{1/3}O_2$ electrode system by combination of soft and hard x-ray absorption spectroscopy. J Am Chem Soc 127:17479–17487
84. Choi J, Manthiram A (2005) Role of chemical and structural stabilities on the electrochemical properties of layered $LiNi_{1/3}Mn_{1/3}Co_{1/3}O_2$ cathodes. J Electrochem Soc 152:A1714–A1718
85. Belharouak I, Lu W, Vissers D, Amine K (2006) Safety characteristics of $Li(Ni_{0.8}Co_{0.15}Al_{0.05})O_2$ and $Li(Ni_{1/3}Co_{1/3}Mn_{1/3})O_2$. Electrochem Commun 8:329–335
86. Ngala JK, Chernova NA, Ma M, Mamak M, Zavalij PY, Whittingham MS (2004) The synthesis, characterization and electrochemical behavior of the layered $LiNi_{0.4}Mn_{0.4}Co_{0.2}O_2$ compound. J Mater Chem 14:214–220
87. Xiao J, Chernova NA, Whittingham MS (2008) Layered mixed transition metal oxide cathodes with reduced cobalt content for lithium ion batteries. Chem Mater 20:7454–7464
88. Chernova NA, Ma M, Xiao J, Whittingham MS, Breger J, Grey CP (2007) Layered $Li_xNi_yMn_yCo_{1-2y}O_2$ cathodes for lithium ion batteries: understanding local structure via magnetic properties. Chem Mater 19:4682–4693
89. Liu D, Wang Z, Chen L (2006) Comparison of structure and electrochemistry of Al- and Fe-doped $LiNi_{1/3}Co_{1/3}Mn_{1/3}O_2$. Electrochim Acta 51:4199–4203
90. Hu S-K, Chou T-C, Hwang B-J, Ceder G (2006) Effect of Co content on performance of $LiAl_{1/3-x}Co_xNi_{1/3}Mn_{1/3}O_2$. J Power Sources 160:1287–1293
91. Zhou F, Zhao X, Lu Z, Jiang J, Dahn JR (2008) The effect of Al substitution on the reactivity of delithiated $LiNi_{1/3}Mn_{1/3}Co_{(1/3-z)}Al_zO_2$ with non-aqueous electrolyte. Electrochem Commun 10:1054–1057
92. Wilcox J, Patoux S, Doeff M (2009) Structure and electrochemistry of $LiNi_{1/3}Co_{1/3-y}M_yMn_{1/3}O_2$ (M = Ti, Al, Fe) positive electrode materials. J Electrochem Soc 156:A192–A198
93. Wilcox JD, Rodriguez EE, Doeff MM (2009) The impact of aluminum and iron substitution on the structure and electrochemistry of $Li(Ni_{0.4}Co_{0.2-y}M_yMn_{0.4})O_2$. J Electrochem Soc 156: A1011–A1018
94. Xiao J, Chernova NA, Whittingham MS (2010) Influence of manganese content on the performance of $LiNi_{0.9-y}Mn_yCo_{0.1}O_2$ ($0.45 \le y \le 0.60$) as a cathode material for li-ion batteries. Chem Mater 22:1180–1185
95. Thackeray MM, Kang S-H, Johnson CS, Vaughey JT, Benedek R, Hackney SA (2007) Li_2MnO_3-stabilized $LiMO_2$ (M=Mn, Ni, Co) electrodes for lithium-ion batteries. J Mater Chem 17:3112–3135
96. Johnson CS, Li N, Lifief C, Thackeray MM (2007) Anomalous capacity and cycling stability of $xLi_2MnO_3 \bullet (1-x)LiMO_2$ electrodes (M=Mn, Ni, Co) in lithium batteries at 50°C. Electrochem Commun 9:787–795
97. Hunter JC (1981) Preparation of a new crystal form of manganese dioxide: λ-MnO_2. J Sol State Chem 32:142–147
98. Thackeray MM, David WIF, Bruce PG, Goodenough JB (1983) Lithium insertion into manganese spinels. Mat Res Bull 18:461–472

99. Goodenough JB, Thackeray MM, David WIF, Bruce PG (1984) Lithium insertion/extraction reactions with manganese oxides. Rev Chim Miner 21:435–455
100. Thackeray MM (1999) Spinel electrodes for lithium batteries. J Am Ceram Soc 82:337–3354
101. Tarascon JM, Wang E, Shokoohi FK, McKinnon WR, Colson S (1991) The spinel phase of $LiMn_2O_4$ as a cathode in secondary lithium cells. J Electrochem Soc 138:2859–2864
102. Tarascon JM, McKinnon WR, Coowar F, Bowmer TN, Amatucci G, Guyomard D (1994) Synthesis conditions and oxygen stoichiometry effects on Li insertion into the spinel $LiMn_2O_4$. J Electrochem Soc 141:1421–1431
103. Guyomard D, Tarascon JM (1994) The carbon/$Li_{1+x}Mn_2O_4$ system. Sol State Ionics 69:222–237
104. Xia Y, Zhou Y, Yoshio M (1997) Capacity fading on cycling of 4 V Li/$LiMn_2O_4$ cells. J Electrochem Soc 144:2593–2600
105. Amatucci G, Tarascon J-M (2002) Optimization of insertion compounds such as $LiMn_2O_4$ for li-ion batteries. J Electrochem Soc 149:K31–K46
106. Gummow RJ, de Kock A, Thackeray MM (1994) Improved capacity retention in rechargeable 4 V lithium/lithium manganese oxide (spinel) cells. Sol State Ionics 69:59–67
107. Shaju KM, Subba Rao GV, Chowdari BVR (2002) Spinel phases, $LiM_{1/6}Mn_{11/6}O_4$ (M=Co, CoAl, CoCr, CrAl), as cathodes for lithium-ion batteries. Sol State Ionics 148:343–350
108. Tucker MC, Reimer JA, Cairns EJ (2002) A 7Li NMR study of capacity fade in metal-substituted lithium manganese oxide spinels. J Electrochem Soc 149:A574–A585
109. Grush MM, Horne CR, Perera RCC, Ederer DL, Cramer SP, Cairns EJ, Callcott TA (2000) Correlating electronic structure with cycling performance of substituted $LiMn_2O_4$ electrode materials: a study using the techniques of soft x-ray absorption and emission. Chem Mater 12:659–664
110. Myung S-T, Komaba S, Kumagai N (2001) Enhanced structural stability and cyclability of Al-doped $LiMn_2O_4$ spinel synthesized by the emulsion drying method. J Electrochem Soc 148:A482–A489
111. Ariyoshi K, Iwata E, Kuniyoshi M, Wakabayashi H, Ohzuku T (2006) Lithium aluminum manganese oxide having spinel framework structure for long-life lithium-ion batteries. Electrochem Sol State Lett 9:A557–A560
112. Amatucci GG, Pereira N, Zheng T, Tarascon J-M (2001) Failure mechanism and improvement of the elevated temperature cycling of $LiMn_2O_4$ compounds through the use of the $LiAl_xMn_{2-x}O_{4-z}F_z$ solid solution. J Electrochem Soc 148:A171–A182
113. Whittingham MS (2004) Lithium batteries and cathode materials. Chem Rev 104:4271–4301
114. Thackeray MM, de Kock A, Rossouw MH, Liles D, Bittihn R, Hoge D (1992) Spinel electrodes from the Li-Mn-O system for rechargeable lithium battery applications. J Electrochem Soc 139:363–366
115. Kim J, Manthiram A (1998) Low temperature synthesis and electrode properties of $Li_4Mn_5O_{12}$. J Electrochem Soc 145:L53–L55
116. Pasquier Du, Blyr A, Courjal P, Larcher D, Amatucci G, Gérand B, Tarascon J-M (1999) Mechanism for limited 55°C storage performance of $Li_{1.05}Mn_{1.95}O_4$ electrodes. J Electrochem Soc 146:428–436
117. Wen SJ, Richardson TJ, Ma L, Striebel KA, Ross PN, Cairns EJ (1996) FTIR spectroscopy of metal oxide insertion electrodes. J Electrochem Soc 143:L136–L138
118. Eriksson T, Gustafsson T, Thomas JO (2002) Surface structure of $LiMn_2O_4$ electrodes. Electrochem Sol State Lett 5:A35–A38
119. Akimoto J, Takahashi Y, Kijima N (2005) Direct observation of the bulk degradation of $Li_{1.1}Mn_{1.9}O_4$ single crystals after high-temperature storage. Electrochem Sol State Lett 8:A361–A364
120. Kobayashi H, Sakaebe H, Komoto K, Kageyama H, Tabuchi M, Tatsumi K, Kohigashi T, Yonemura M, Kanno R, Kamiyama T (2003) Structure and physical property changes of delithiated spinels for $Li_{1.02-x}Mn_{1.98}O_4$ after high-temperature storage. Sol State Ionics 156:309–318

121. Quinlan FT, Sano K, Willey T, Vidu R, Tasaki K, Stroeve P (2001) Surface characterization of the spinel $Li_xMn_2O_4$ cathode before and after storage at elevated temperatures. Chem Mater 13:4207–4212
122. Tsunekawa H, Tanimoto S, Marubayashi R, Fujita M, Kifune K, Sano M (2002) Capacity fading of graphite electrodes due to the deposition of manganese ions on them in Li-ion batteries. J Electrochem Soc 149:A1326–A1331
123. Amine K, Liu J, Kang S, Belharouak I, Hyung Y, Vissers D, Henriksen G (2004) Improved lithium manganese oxide spinel/graphite Li-ion cells for high-power applications. J Power Sources 129:14–19
124. Cho J, Kim GB, Lim HS, Kim C-S, Yoo S-I (1999) Improvement of structural stability of $LiMn_2O_4$ cathode material on 55°C cycling by sol-gel coating of $LiCoO_2$. Electrochem Sol State Lett 2:607–609
125. Wang EI (1998) Method of treating lithium manganese oxide spinel. US Patent 5,783,328
126. Xu W, Angell CA (2001) LiBOB and its derivatives weakly coordinating anions, and the exceptional conductivity of their nonaqueous solutions. Electrochem Sol State Lett 4:E1–E4
127. Xu K, Zhang S, Jow TR, Xu W, Angell CA (2002) LiBOB as salt for lithium-ion batteries a possible solution for high temperature operation. Electrochem Solid State Lett 5(1): A26–A29
128. Chen Z, Amine K (2006) Capacity fade of $Li_{1+x}Mn_{2-x}O_4$-based lithium-ion cells. J Electrochem Soc 153:A316–A320
129. Kitao H, Fujihara T, Takeda K, Nakanishi N, Nohma T (2005) High-temperature storage performance of Li-ion batteries using a mixture of Li-Mn spinel and Li-Ni-Co-Mn oxide as a positive electrode material. Electrochem Sol State Lett 8:A87–A90
130. MacNeil DD, Dahn JR (2001) The reaction of charged cathodes with nonaqueous solvents and electrolytes II. $LiMn_2O_4$ charged to 4.2 V. J Electrochem Soc 148:A1211–A1215
131. Thackeray MM (1995) Structural considerations of layered and spinel lithiated oxides for lithium ion batteries. J Electrochem Soc 142:2558–2563
132. Sigala C, Guyomard D, Verbaere A, Piffard Y, Tournoux M (1995) Positive electrode materials with high operating voltage for lithium batteries: $LiCr_yMn_{2-y}O_4$ ($0 \leq y \leq 1$). Sol State Ionics 81:167–170
133. Kawai H, Nagata M, Tabuchi M, Tukamoto H, West AR (1998) Novel 5V spinel cathode $Li_2FeMn_3O_8$ for lithium ion batteries. Chem Mater 10:3266–3268
134. Ein-Eli Y, Howard WF (1997) $LiCu_x{}^{II}Cu_y{}^{III}Mn_{[2-(x+y)]}{}^{III,\ IV}O_4$: 5V cathode materials. J Electrochem Soc 144:L205–L207
135. Kawai H, Nagata M, Tukamoto H, West AR (1998) A novel cathode $Li_2CoMn_3O_8$ for lithium ion batteries operating over 5V. J Mater Chem 8:837–839
136. Zhong Q, Bonakdarpour A, Zhang M, Gao Y, Dahn JR (1997) Synthesis and electrochemistry of $LiNi_xMn_{2-x}O_4$. J Electrochem Soc 144:205–213
137. Ohzuku T, Takeda S, Iwanaga M (1999) Solid-state redox potentials for $Li[Me_{1/2}Mn_{3/2}]O_4$ (Me: 3d-transition metal) having spinel-framework structures: a series of 5 volt materials for advanced lithium-ion batteries. J Power Sources 81–82:90–94
138. Sun Y-K, Lee Y-S, Yoshio M, Amine K (2002) Synthesis and electrochemical properties of ZnO-coated $LiNi_{0.5}Mn_{1.5}O_4$ spinel as 5V cathode material for lithium secondary batteries. Electrochem Sol State Lett 5:A99–A102
139. Liu J, Manthiram A (2009) Kinetics study of the 5V spinel cathode $LiMn_{1.5}Ni_{0.5}O_4$ before and after surface modifications. J Electrochem Soc 156:A833–A838
140. Patoux S, Daniel L, Bourbon C, Lignier H, Pagano C, Le Cras F, Jouanneau S, Martinet S (2009) High voltage spinel oxides for Li-ion batteries: from the materials research to the application. J Power Sources 189:344–352
141. Kim J-H, Myung S-T, Yoon CS, Oh I-H, Sun Y-K (2004) Effect of Ti substitution of $LiNi_{0.5}Mn_{1.5-x}Ti_xO_4$ and their electrochemical properties as lithium insertion material. J Electrochem Soc 151:A1911–A1918

142. Arunkumar TA, Manthiram A (2005) Influence of lattice parameter differences on the electrochemical performance of the 5V spinel $LiMn_{1.5-y}Ni_{0.5-z}M_{y+z}O_4$ (M=Li, Mg, Fe, Co, and Zn). Electrochem Sol State Lett 8:A403–A405
143. Ooms FGB, Kelder EM, Schoonman J, Wagemaker M, Mulder FM (2002) High-voltage $LiMg_{\delta}Ni_{0.5-\delta}Mn_{1.5}O_4$ spinels for Li-ion batteries. Sol State Ionics 152–153:143–153
144. Gryffoy D, Vandenberghe RE, Legrand E (1991) A neutron diffraction study of some spinel compounds containing octahedral Ni and Mn at a 1:3 ratio. Mater Sci Forum 79–82:785–790
145. Takahashi K, Saitoh M, Sano M, Fujita M, Kifune K (2004) Electrochemical and structural properties of a 4.7V-class $LiNi_{0.5}Mn_{1.5}O_4$ positive electrode material prepared with a self-reaction method. J Electrochem Soc 151:A173–A177
146. Kunduraci M, Amatucci GG (2006) Synthesis and characterization of nanostructured 4.7V $Li_xMn_{1.5}Ni_{0.5}O_4$ spinels for high-power lithium-ion batteries. J Electrochem Soc 153: A1345–A1352
147. Wu HM, Belharouak I, Deng H, Abouimrane A, Sun Y-K, Amine K (2009) Development of $LiNi_{0.5}Mn_{1.5}O_4/Li_4Ti_5O_{12}$ system with long cycle life. J Electrochem Soc 156:A1047–A1050
148. Padhi AK, Nanjundaswamy KS, Goodenough JB (1997) Phospho-olivines as positive-electrode materials for rechargeable lithium batteries. J Electrochem Soc 144:1188–1194
149. Andersson AS, Kalska B, Häggstrom L, Thomas JO (2000) Lithium extraction/insertion in $LiFePO_4$: an x-ray diffraction and Mössbauer spectroscopy study. Sol State Ionics 130:41–52
150. Tarascon J-M, Armand M (2001) Issues and challenges facing rechargeable lithium batteries. Nature 414:359–376
151. Ravet N, Chouinard Y, Magnan JF, Besner S, Gauthier M, Armand M (2001) Electroactivity of natural and synthetic triphylite. J Power Sources 97–98:503–507
152. Barker J, Saidi MY, Swoyer JL (2003) A carbothermal reduction method for the preparation of electroactive materials for lithium ion applications. J Electrochem Soc 150:A684–A688
153. Doeff MM, Wilcox JD, Kostecki R, Lau G (2006) Optimization of carbon coatings on $LiFePO_4$. J Power Sources 163:180–184
154. Dominko R, Bele M, Gaberscek M, Remskar M, Hanzel D, Pejovnik S, Jamnik J (2005) Impact of the carbon coating thickness on the electrochemical performance of $LiFePO_4/C$ composites. J Electrochem Soc 152:A607–A610
155. Huang H, Yin S-C, Nazar LF (2001) Approaching theoretical capacity of $LiFePO_4$ at room temperature at high rates. Electrochem Sol State Lett 4:A170–A172
156. Doeff MM, Hu Y, McLarnon F, Kostecki R (2003) Effect of surface carbon structure on the electrochemical performance of $LiFePO_4$. Electrochem Sol State Lett 6:A207–A209
157. Zaghib K, Shim J, Guerfi A, Charest P, Striebel KA (2005) Effect of carbon source as additives in $LiFePO_4$ as positive electrode for li-ion batteries. Electrochem Sol State Lett 8: A207–A210
158. Wilcox JD, Doeff MM, Marcinek M, Kostecki R (2007) Factors influencing the quality of carbon coatings on $LiFePO_4$. J Electrochem Soc 154:A389–A395
159. Doeff MM, Wilcox JD, Yu R, Aumentado A, Marcinek M, Kostecki R (2008) Impact of carbon structure and morphology on the electrochemical performance of $LiFePO_4/C$ composites. J Sol State Electrochem 12:995–1001
160. Chen Z, Dahn JR (2002) Reducing carbon in $LiFePO_4/C$ composite electrodes to maximize specific energy, volumetric energy, and tap density. J Electrochem Soc 149:A1184–A1189
161. Chung S-Y, Bloking JT, Chiang Y-M (2002) Electronically conductive phospho-olivines as lithium storage electrodes. Nat Mater 1:123–128
162. Thackeray MM (2002) An unexpected conductor. Nat Mater 1:81–82
163. Ravet N, Abouimrane A, Armand M (2003) From our readers. Nat Mater 2:702–703
164. Herle PS, Ellis B, Coombs N, Nazar LF (2004) Nano-network electronic conduction in iron and nickel olivine phosphates. Nat Mater 3:147–152
165. Delacourt C, Wurm C, Laffont L, Leriche J-B, Masquelier C (2006) Electrochemical and electrical properties of Nb- and/or C-containing $LiFePO_4$ composites. Sol State Ionics 177:333–341

166. Rho Y-H, Nazar LF, Perry L, Ryan D (2007) Surface chemistry of $LiFePO_4$ studied by Mössbauer and x-ray photoelectron spectroscopy and its effect on electrochemical properties. J Electrochem Soc 154:A283–A289
167. Wagemaker M, Ellis BL, Lützenkirchen-Hecht D, Mulder FM, Nazar LF (2008) Proof of supervalent doping in olivine $LiFePO_4$. Chem Mater 20:6313–6315
168. Islam MS, Driscoll DJ, Fisher CAJ, Slater PR (2005) Atomic-scale investigation of defects, dopants, and lithium transport in the $LiFePO_4$ olivine-type battery material. Chem Mater 17:5085–5092
169. Maier J, Amin R (2008) Defect chemistry of $LiFePO_4$. J Electrochem Soc 155:A339–A344
170. Axmann P, Stinner C, Wohlfahrt-Mehrens M, Mauger A, Gendron G, Julien CM (2009) Nonstoichiometric $LiFePO_4$: defects and related properties. Chem Mater 21:1636–1644
171. Amin R, Maier J (2008) Effect of annealing on transport properties of $LiFePO_4$: towards a defect chemical model. Sol State Ionics 178:1831–1836
172. Morgan D, Van der Ven A, Ceder G (2004) Li conductivity in Li_xMPO_4 (M=Mn, Fe, Co, Ni) olivine materials. Electrochem and Sol State Lett 7:A30–A32
173. Li J, Yao W, Martin S, Vaknin D (2008) Lithium ion conductivity in single crystal $LiFePO_4$. Sol State Ionics 179:2016–2019
174. Amin R, Maier J, Balaya P, Chen DP, Lin CT (2008) Ionic and electronic transport in single crystalline $LiFePO_4$ grown by optical floating zone technique. Sol State Ionics 179:1683–1687
175. Gardiner GR, Islam MS (2010) Anti-site defects and ion migration in the $LiFe_{0.5}Mn_{0.5}PO_4$ mixed-metal cathode material. Chem Mater 22:1242–1248
176. Chen J, Vacchio MJ, Wang S, Chernova N, Zavalij PY, Whittingham MS (2008) The hydrothermal synthesis and characterization of olivines and related compounds for electrochemical applications. Sol State Ionics 178:1676–1693
177. Delacourt C, Poizot P, Levasseur S, Masquelier C (2006) Size effects on carbon-free $LiFePO_4$ powders the key to superior energy density. Electrochem Sol State Lett 9:A352–A355
178. Meethong N, Huang H-YS, Carter WC, Chiang Y-M (2007) Size-dependent lithium miscibility gap in nanoscale $Li_{1-x}FePO_4$. Electrochem Sol State Lett 10:A134–A138
179. Gibot P, Casas-Cabanas M, Laffont L, Levasseur S, Carlach P, Hamelet S, Tarascon J-M, Masquelier C (2008) Room-temperature single-phase Li insertion/extraction in nanoscale Li_xFePO_4. Nat Mater 7:741–747
180. Yamada A, Koizumi H, Sonoyama N, Kanno R (2005) Phase change in Li_xFePO_4. Electrochem Sol State Lett 8:A409–A413
181. Yamada A, Koizumi H, Nishimura S-I, Sonoyama N, Kanno R, Yonemura M, Nakamura T, Kobayashi Y (2006) Room-temperature miscibility gap in Li_xFePO_4. Nat Mater 5:357–360
182. Hamelet S, Gibot P, Casas-Cabanas M, Bonnin D, Grey CP, Cabana J, Leriche J-B, Rodriguez-Carvajal CM, Levasseur S, Carlach P, Van Thournout M, Tarascon J-M, Masquelier C (2009) The effects of moderate thermal treatments under air on $LiFePO_4$-based nano powders. J Mater Chem 19:3979–3991
183. Yu DYW, Donoue K, Kadohata T, Murata T, Matsuta S, Fujitani S (2008) Impurities in $LiFePO_4$ and their influence on material characteristics. J Electrochem Soc 155:A526–A530
184. Dokko K, Shiraishi K, Kanamura K (2005) Identification of surface impurities on $LiFePO_4$ particles prepared by a hydrothermal process. J Electrochem Soc 152:A2199–A2202
185. Delacourt C, Poizot P, Tarascon J-M, Masquelier C (2005) The existence of a temperature-driven solid solution in Li_xFePO_4 for $0 \leq x \leq 1$. Nat Mater 4:254–260
186. Dodd JL, Yazami R, Fultz B (2006) Phase diagram of Li_xFePO_4. Electrochem Sol State Lett 9:A151–A155
187. Chen G, Song X, Richardson TJ (2007) Metastable solid-solution phases in the $LiFePO_4$/$FePO_4$ system. J Electrochem Soc 154:A627–A632
188. Srinivasan V, Newman J (2004) Discharge model for the lithium iron-phosphate electrode. J Electrochem Soc 151:A1517–A1529

189. Chen G, Song X, Richardson TJ (2006) Electron microscopy study of the $LiFePO_4$ to $FePO_4$ phase transition. Electrochem Sol State Lett 9:A295–A298
190. Andersson AS, Thomas JO (2001) The source of first cycle capacity loss in $LiFePO_4$. J Power Sources 97–98:498–502
191. Laffont L, Delacourt C, Gibot P, Wu MY, Kooyman P, Masquelier C, Tarascon JM (2006) Study of the $LiFePO_4/FePO_4$ two-phase system by high-resolution electron energy loss spectroscopy. Chem Mater 18:5520–5529
192. Delmas C, Maccario M, Croguennec L, Le Cras F, Weill F (2008) Lithium deintercalation in $LiFePO_4$ nanoparticles via a domino-cascade model. Nat Mater 7:665–671
193. Allen JL, Jow TR, Wolfenstine J (2007) Kinetic study of the electrochemical $FePO_4$ to $LiFePO_4$ phase transition. Chem Mater 19:2108–2111
194. Lee KT, Kan WH, Nazar LF (2009) Proof of intercrystallite ionic transport in $LiMPO_4$ electrodes (M=Fe, Mn). J Am Chem Soc 131:6044–6045
195. Kang B, Ceder G (2009) Battery materials for ultrafast charging and discharging. Nature 458:190–193
196. Amine K, Liu J, Belharouak I (2005) High-temperature storage and cycling of C-$LiFePO_4$/graphite Li-ion cells. Electrochem Commun 7:669–673
197. Koltypin M, Aurbach D, Nazar L, Ellis B (2007) On the stability of $LiFePO_4$ olivine cathodes under various conditions (electrolyte solutions, temperatures). Electrochem Solid-State Lett 10:A40–A44
198. Yang S, Song Y, Zavalij PY, Whittingham MS (2002) Reactivity, stability and electrochemical behavior of lithium iron phosphates. Electrochem Commun 4:239–244
199. Li G, Azuma H, Tohda M (2002) $LiMnPO_4$ as the cathode for lithium batteries. Electrochem Sol State Lett 5:A135–A137
200. Rissouli K, Benkhouja K, Ramos-Barrado JR, Julien C (2003) Electrochemical conductivity in lithium orthophosphates. Mater Sci Eng B 98:185–189
201. Delacourt C, Laffont L, Bouchet R, Wurm C, Leriche J-B, Morcrette M, Tarascon J-M, Masquelier C (2005) Toward understanding of electrical limitations (electronic, ionic) in $LiMPO_4$ (M=Fe, Mn) electrode materials. J Electrochem Soc 152:A913–A921
202. Delacourt C, Poizot P, Morcrette M, Tarascon J-M, Masquelier C (2004) One step low-temperature route for the preparation of electrochemically active $LiMnPO_4$ powders. Chem Mater 16:93–99
203. Yang J, Xu JJ (2006) Synthesis and characterization of carbon-coated lithium transition metal phosphates $LiMPO_4$ (M=Fe, Mn, Co, Ni) prepared via a nonaqueous sol-gel route. J Electrochem Soc 153:A716–A723
204. Kwon N-H, Drezen T, Exnar I, Teerlinck I, Isono M, Graetzel M (2006) Enhanced electrochemical performance of mesoparticulate $LiMnPO_4$ for lithium ion batteries. Electrochem and Solid State Lett 9:A277–A280
205. Kim TR, Kim DH, Ryu HW, Moon JH, Lee JH, Boo S, Kim J (2007) Synthesis of lithium manganese phosphate nanoparticle and its properties. J Phys Chem Sol 68:1203–1206
206. Bakenov Z, Taniguchi I (2010) Electrochemical performance of nanocomposite $LiMnPO_4$/C cathode materials for lithium batteries. Electrochemistry Commun 12:75–78
207. Xiao J, Xu W, Choi D, Zhang J-G (2010) Synthesis and characterization of lithium manganese phosphate by a precipitation method. J Electrochem Soc 157:A142–A147
208. Doeff MM, Chen J, Conry TE, Wang R, Wilcox J, Aumentado A (2010) Combustion synthesis of nanoparticulate $LiMg_xMn_{1-x}PO_4$ (x = 0, 0.1, 0.2) carbon composites. J Mater Res 25:1460–1468
209. Drezen T, Kwon N-H, Bowen P, Terrlinck I, Isono M, Exnar I (2007) Effect of particle size on $LiMnPO_4$ cathodes. J Power Sources 174:949–953
210. Chen G, Wilcox JD, Richardson TJ (2008) Improving the performance of lithium manganese phosphate through divalent cation substitution. Electrochem Sol State Lett 11:A190–A194

211. Shiratsuchi T, Okada S, Doi T, Yamaki J-I (2009) Cathodic performance of $LiMn_{1-x}M_xPO_4$ (M = Ti, Mg, and Zr) annealed in an inert atmosphere. Electrochim Acta 54:3145–3151
212. Bakenov Z, Taniguchi I (2010) $LiMg_xMn_{1-x}PO_4/C$ cathodes for lithium batteries prepared by a combination of spray pyrolysis with wet ballmilling. J Electrochem Soc 157:A430–A436
213. Martha SK, Markovsky B, Grinblat J, Gofer Y, Haik O, Zinigrad E, Aurbach D, Drezen T, Wang D, Deghenghi G, Exnar I (2009) $LiMnPO_4$ as an advanced cathode material for rechargeable lithium batteries. J Electrochem Soc 156:A541–A552
214. Yonemura M, Yamada A, Takei Y, Sonoyama N, Kanno R (2004) Comparative kinetic study of olivine Li_xMPO_4 (M=Fe, Mn). J Electrochem Soc 151:A1352–A1356
215. Yamada A, Chung S-C (2001) Crystal chemistry of the olivine-type $Li(Mn_yFe_{1-y})PO_4$ and $(Mn_yFe_{1-y})PO_4$ as possible 4 V cathode materials for lithium batteries. J Electrochem Soc 148:A960–A967
216. Chen G, Richardson TJ (2009) Solid solution phases in the olivine-type $LiMnPO_4/MnPO_4$ system. J Electrochem Soc 156:A756–A762
217. Kim S-W, Kim J, Gwon H, Kang K (2009) Phase stability study of $Li_{1-x}MnPO_4$ ($0 \leq x \leq 1$) cathode for Li rechargeable battery. J Electrochem Soc 156:A635–A638
218. Chen G, Richardson TJ (2010) Thermal instability of olivine-type $LiMnPO_4$ cathodes. J Power Sources 195:1221–1224
219. Okada S, Sawa S, Egashira M, Yamaki J-I, Tabuchi M, Kageyama H, Konishi T, Yoshino A (2001) Cathode properties of phospho-olivine $LiMPO_4$ for lithium secondary batteries. J Power Sources 97–98:430–432
220. Wolfenstine J, Allen J (2004) $LiNiPO_4$–$LiCoPO_4$ solid solutions as cathodes. J Power Sources 136:150–153
221. Deniard P, Dulac AM, Rocquefelte X, Grigorova V, Lebacq O, Pasturel A, Jobic S (2004) High potential positive materials for lithium-ion batteries: transition metal phosphates. J Phys Chem Sol 65:229–233
222. Chang X-Y, Wang Z-X, Li X-H, Zhang L, Guo H-J, Peng W-J (2005) Synthesis and performance of $LiMn_{0.7}Fe_{0.3}PO_4$ cathode material for lithium ion batteries. Mater Res Bull 40:1513–1520
223. Yamada A, Kudo Y, Liu K-Y (2001) Phase diagram of $Li_x(Mn_yFe_{1-y})PO_4$ ($0 \leq x, y \leq 1$). J Electrochem Soc 148:A1153–A1158
224. Bramnik NN, Bramnik KG, Nikolowski K, Hinterstein M, Baehtz C, Ehrenbert H (2005) Synchrotron diffraction study of lithium extraction from $LiMn_{0.6}Fe_{0.4}PO_4$. Electrochem Sol State Lett 8:A379–A381
225. Park Y-U, Kim J, Gwon H, Seo D-H, Kim S-W, Kang K (2010) Synthesis of multicomponent olivine by a novel mixed transition metal oxalate coprecipitation method and electrochemical characterization. Chem Mater 22:2573–2581
226. Gwon H, Seo D-H, Kim S-W, Kim J, Kang K (2009) Combined first-principle calculations and experimental study on multi-component olivine cathode for lithium rechargeable batteries. Adv Funct Mater 19:1–8
227. Seo D-H, Gwon H, Kim S-W, Kim J, Kang K (2010) Multicomponent olivine cathode for lithium rechargeable batteries: a first-principles study. Chem Mater 22:518–523
228. Goodenough JB, Hong Y-P, Kafalas JA (1976) Fast Na^+-ion transport in skeleton structures. Mater Res Bull 11:203–220
229. Delmas C, Nadiri A (1988) The Nasicon-type titanium phosphates $ATi_2(PO_4)_3$ (A=Li, Na) as electrode materials. Sol State Ionics 28–30:419–423
230. Delmas C, Cherkaoui F, Nadiri A, Hagenmuller P (1987) A Nasicon-type phase as intercalation electrode: $NaTi_2(PO_4)_3$. Mat Res Bull 22:631–639
231. Manthiram A, Goodenough JB (1989) Lithium insertion into $Fe_2(SO_4)_3$ frameworks. J Power Sources 26:403–408
232. Nanjundaswamy KS, Padhi AK, Goodenough JB, Okada S, Ohtsuka H, Arai H, Yamaki J (1996) Synthesis, redox potential evaluation and electrochemical characteristics of NASICON-related-3D framework compounds. Sol State Ionics 92:1–10

233. Masquelier C, Padhi AK, Nanjundaswamy KS, Goodenough JB (1998) New cathode materials for rechargeable lithium batteries: the 3-D framework structures $Li_3Fe_2(XO_4)_3$ (X=P, As). J Sol State Chem 135:228–234
234. Saïdi MY, Barker J, Huang H, Swoyer JL, Adamson G (2002) Electrochemical properties of lithium vanadium phosphate as a cathode material for lithium-ion batteries. Electrochem Sol State Lett 5:A149–A151
235. Morcrette M, Leriche J-B, Patoux S, Wurm C, Masquelier C (2003) In situ x-ray diffraction during lithium extraction from rhombohedral and monoclinic $Li_3V_2(PO_4)_3$. Electrochem Sol State Lett 6:A80–A84
236. Yin S-C, Strobel PS, Grondey H, Nazar LF (2004) $Li_{2.5}V_2(PO_4)_3$: a room-temperature analogue to the fast-ion conducting high-temperature γ-phase of $Li_3V_2(PO_4)_3$. Chem Mater 16:1456–1465
237. Gover RKB, Burns P, Bryan A, Saidi MY, Swoyer JL, Barker J (2006) $LiVPO_4F$: A new active material for safe lithium-ion batteries. Sol State Ionics 177:2635–2638
238. Barker J, Gover RKB, Burns P, Bryan A, Saidi MY, Swoyer JL (2005) Structural and electrochemical properties of lithium vanadium fluorophosphate, $LiVPO_4F$. J Power Sources 146:516–520
239. Barker J, Gover RKB, Burns P, Bryan A (2005) A symmetrical lithium-ion cell based on lithium vanadium fluorophosphate, $LiVPO_4F$. Electrochem Sol State Lett 8:A285–A287
240. Gover RKB, Bryan A, Burns P, Barker J (2006) The electrochemical insertion properties of sodium vanadium fluorophosphate, $Na_3V_2(PO_4)_2F_3$. Sol State Ionics 177:1495–1500
241. Ellis BL, Makahnouk WRM, Makimura Y, Toghill K, Nazar LF (2007) A multifunctional 3.5 V iron-based phosphate cathode for rechargeable batteries. Nat Mater 6:749–753
242. Ramesh TN, Lee KT, Ellis BL, Nazar LF (2010) Tavorite lithium iron fluorophosphate cathode materials: phase transition and electrochemistry of $LiFePO_4F$–Li_2FePO_4F. Electrochem Sol State Lett 13:A43–A47
243. Recham N, Chotard J-N, Jumas J-C, Laffont L, Armand M, Tarascon J-M (2010) Ionothermal synthesis of Li-based fluorophosphates electrodes. Chem Mater 22:1142–1148
244. Song Y, Zavalij PY, Chernova NA, Whittingham MS (2005) Synthesis, crystal structure, and electrochemical and magnetic study of new iron (III) hydroxyl-phosphates, isostructural with lipscombite. Chem Mater 17:1139–1147
245. Marx N, Croguennec L, Carlier D, Bourgeois L, Kubiak P, Le Cras F, Delmas C (2010) Structural and electrochemical study of a new crystalline hydrated iron(III) phosphate $FePO_4{\cdot}H_2O$ obtained from $LiFePO_4(OH)$ by ion exchange. Chem Mater 22:1854–1861
246. Gaubicher J, Le Mercier T, Chabre Y, Angenault J, Quarton M (1999) Li/β-$VOPO_4$: a new 4V system for lithium batteries. J Electrochem Soc 146:4375–4379
247. Kerr TA, Gaubicher J, Nazar LF (2000) Highly reversible Li insertion at 4V in ε-$VOPO_4$/α-$LiVPO_4$ cathodes. Electrochem Sol State Lett 3:460–462
248. Song Y, Zavalij PY, Whittingham MS (2005) ε-$VOPO_4$: electrochemical synthesis and enhanced cathode behavior. J Electrochem Soc 152:A721–A727
249. Barker J, Gover RKB, Burns P, Bryan A (2005) $LiVP_2O_7$: a viable lithium-ion cathode material? Electrochem Sol State Lett 8:A446–A448
250. Nytén A, Abouimrane A, Armand M, Gustafsson T, Thomas JO (2005) Electrochemical performance of Li_2FeSiO_4 as a new Li-battery cathode material. Electrochem Commun 7:156–160
251. Dominko R, Bele M, Gaberscek M, Meden A, Remskar M, Jamnik J (2006) Structure and electrochemical performance of Li_2MnSiO_4 and Li_2FeSiO_4 as potential Li-battery cathode materials. Electrochem Commun 8:217–222
252. Gong ZL, Li YX, Yang Y (2006) Synthesis and characterization of $Li_2Mn_xFe_{1-x}SiO_4$ as a cathode material for lithium ion batteries. Electrochem Sol State Lett 9:A542–A544
253. Belharouak I, Abouimrane A, Amine K (2009) Structural and electrochemical characterization of Li_2MnSiO_4 cathode material. J Phys Chem C 113:20733–20737

254. Lyness C, Delobel B, Armstrong AR, Bruce PG (2007) The lithium intercalation compound Li_2CoSiO_4 and its behaviour as a positive electrode for lithium batteries. J Chem Soc Chem Commun 46:4890–4892
255. Armstrong AR, Lyness C, Ménétrier M, Bruce PG (2010) Structural polymorphism in Li_2CoSiO_4 intercalation electrodes: a combined diffraction and NMR study. Chem Mater 22:1892–1900
256. Dominko R (2010) Silicates and titanates as high-energy cathode materials for Li-ion batteries. In: Proceedings of SPIE: energy harvesting and storage: materials, devices and applications II, Orlando
257. Zaghib K, Salah AA, Ravet N, Mauger A, Gendron F, Julien CM (2006) Structural, magnetic and electrochemical properties of lithium iron orthosilicate. J Power Sources 160:1381–1386
258. Nishimura S-I, Hayase S, Kanno R, Yashima M, Nakayama N, Yamada A (2008) Structure of Li_2FeSiO_4. J Am Chem Soc 130:13212–13213
259. Arroyo-de Dompablo ME, Armand M, Tarascon JM, Amador U (2006) On-demand design of polyoxianionic cathode materials based of electronegativity correlations: an exploration of the Li_2MSiO_4 system (M=Fe, Mn, Co, Ni). Electrochem Commun 8:1292–1298
260. Li H, Balaya P, Maier J (2004) Li-storage via heterogeneous reaction in selected binary metal fluorides and oxides. J Electrochem Soc 151:A1878–A1885
261. Bervas M, Mansour AN, Yoon W-S, Al-Sharab JF, Badway F, Cosandey F, Klein LC, Amatucci GG (2006) Investigation of the lithiation and delithiation conversion mechanisms of bismuth fluoride nanocomposites. J Electrochem Soc 153:A799–A808
262. Aurbach D (2000) Review of selected electrode-solution interactions which determine the performance of Li and Li ion batteries. J Power Sources 89:206–218
263. Jaiswal A, Horne CR, Chang O, Zhang W, Kong W, Wang E, Chern T, Doeff MM (2009) Nanoscale $LiFePO_4$ and $Li_4Ti_5O_{12}$ for high rate Li-ion batteries. J Electrochem Soc 156:A1041–A1046
264. Ren Y, Armstrong AR, Jiao F, Bruce PG (2010) Influence of size on the rate of mesoporous electrodes for lithium batteries. J Am Chem Soc 132:996–1004
265. Sun Y-K, Myung S-T, Park B-C, Prakash J, Belharouak I, Amine K (2009) High energy cathode material for long-life and safe lithium batteries. Nat Mater 8:320–324

Books and Reviews

Ammundsen B, Paulsen J (2001) Novel lithium-ion cathode materials based on layered manganese oxides. Adv Mater 13:943–956

Brodd RJ, Bullock KR, Leising RA, Middaugh RL, Miller JR, Takeuchi E (2004) Batteries, 1977 to 2002. J Electrochem Soc 151:K1–K11

Bruce PG (2008) Energy storage beyond the horizon: rechargeable lithium batteries. Solid State Ionics 179:752–760

Ellis BL, Lee KT, Nazar LF (2010) Positive electrode materials for Li-ion and Li batteries. Chem Mater 22:691–714

Fergus JW (2010) Recent developments in cathode materials for lithium ion batteries. J Power Sources 195:939–954

Goodenough JB, Kim Y (2010) Challenges for rechargeable Li batteries. Chem Mater 22:587–603

Huggins RA (2009) Advanced batteries, materials sciences aspects. Springer, New York

Nazri GA, Pistoia O (eds) (2003) Lithium batteries: science and technology. Kluwer, Norwell

Ohzuku T, Brodd RJ (2007) An overview of positive-electrode materials for advanced lithium-ion batteries. J Power Sources 174:449–456

Palacin MR (2009) Recent advances in rechargeable battery materials: a chemist's perspective. Chem Soc Rev 38:2565–2575

Tarascon J-M (2010) Key challenges in future Li-battery research. Phil Trans R Soc Lond A 368:3227–3241

Yamada A, Hosoya M, Chung S-C, Kudo Y, Hinokuma K, Liu K-Y, Nishi Y (2003) Olivine-type cathodes achievements and problems. J Power Sources 119–121:232–238

http://www.springer.com/978-1-4614-5790-9

Batteries for Sustainability
Selected Entries from the Encyclopedia of Sustainability
Science and Technology
Brodd, R.J. (Ed.)
2013, VI, 514 p., Hardcover

ISBN: 978-1-4614-5790-9